replaced, and in some cases, closed lavage was performed with 500 to 3000 mL of natural saline solution, depending on the amylase level in the drained fluid. On developing POPF, all attempts were made to maintain per os and enteral feeding. All patients with obstructive jaundice first underwent endoscopic nasogastric/retrograde bile drainage or percutaneous transhepatic drainage, and it was performed in 61% of patients. All patients received prophylactic antibiotics intraoperatively and for 1 or 2 days postoperatively. The nasogastric tube was routinely removed on postoperative day (POD) 1 after confirmation that the volume of drainage fluid was less than 200 mL/d. Postoperative enteral nutrition through a jejunostomy tube was initiated at POD 3 in all patients. Oral food intake was initiated at POD 5 or 6. Once the patient was getting 50% of required nutrition from an oral diet, enteral nutrition was stopped, and the jejunostomy tube was finally withdrawn at POD 21 at an outpatient clinic. Peripancreatic drainage fluid was collected, and the amylase level was measured and monitored on PODs 3 and 6 and every 3 days thereafter as needed. The date of discharge from hospital was decided by the senior surgeons and was taken once the patient could take more than 50% of solid food served and was afebrile with falling C-reactive protein levels less than 5 mg/dL. No patients had prophylactic octreotide to prevent POPF development and thromboembolic prophylaxis with low-molecular-weight heparin. All complications were prospectively recorded into a prospective pancreatic database.

Group A

Group A consisted of 51 consecutive patients who underwent PD from June 2004 to August 2006; in these patients, the semiclosed external stenting of pancreatic and biliary ducts (polyethylene tube; Sumitomo Bakelite Co, Tokyo, Japan) was used in cases with a pancreatic duct of less than 3 mm in diameter (16 patients, 31%) and with a bile duct of less than 10 mm in diameter (13 patients, 25%). This group has the same population as presented in the previous article.[9]

Group B

Group B consisted of consecutive 78 patients who underwent PD from September 2006 to September 2008. All patients underwent PJ without external stenting of the pancreatic and biliary duct. In this group, 36 patients (46%) had a pancreatic duct of less than 3 mm in diameter.

Definition of Postoperative Complications

The overall general and surgery-related complications were recorded in this study. These included delayed gastric emptying, POPF, wound dehiscence, intra-abdominal infection, abdominal abscess formation, cardiopulmonary disorder, hemorrhagic complication, peritoneal/pleural effusion, anastomotic leakage, marginal ulcer formation, and diarrhea and other complications. Each day that a patient demonstrated clinical symptoms of SIRS[15] was recorded. Sepsis was considered to be present if a patient had any complication involving clinical symptoms of infection-induced SIRS that continued for more than 2 inpatient days. Clinical symptoms of SIRS within the first 4 PODs were excluded as a systemic response to surgical stress.

The POPF was defined according to the International Study group of Pancreatic Fistula criteria.[16] Abdominal abscess, including liver abscess, was defined as a collection of pus or infected fluid confirmed by ultrasound, computed tomography–guided aspiration and culture, or a second laparotomy. Delayed gastric emptying was defined according to the International Study Group of Pancreatic Surgery.[17] Wound dehiscence was diagnosed as an open wound with or without the clinical presence of pus or microbiological findings of bacteria. Intra-abdominal infection was regarded as radiological findings of fluid collection (pleural effusion and/or ascites) or microbiological findings of bacteria with infection-induced SIRS. Peritoneal/pleural effusion was defined as more than 200 mL/d of drained fluid beyond the 14th POD. Anastomotic leakage was radiologically diagnosed by leakage of contrast agents from the anastomosis. Upper gastrointestinal endoscopy for marginal ulcer formation was performed when patients showed signs of appetite loss, epigastralgia, or bloody discharge from the nasogastric tube or in the stools. Hemorrhagic complication was defined as intra-abdominal or intestinal bleeding requiring blood transfusion, operation, and/or radiological intervention. Aspartate aminotransferase or alanine aminotransferase levels of more than twice the upper limit of normal reference indicated postoperative liver dysfunction, including cholangitis. Death of a patient for any reason was regarded as in-hospital death.

Statistical Analysis

Mortality and morbidity after PD were calculated for each group and were compared between groups A and B. Patient variables included age, sex, clinical diagnosis, comorbid disease, obstructive jaundice, operative variables, preoperative blood tests, and preoperative chemoradiation. Operative variables included the type and duration of operation, estimated blood loss, type of blood transfusion, and extent of operation, including resection of adjacent organs and portal vein. All data were entered into an electronic database on a personal computer, and continuous variables are expressed as median values and ranges. Statistical analyses including Mann-Whitney U test and Fisher exact test were performed using StatView Version 5.0 for Windows (SAS, Inc, Cary, NC). The profound factors identified by the univariate analysis were further examined by multivariate analysis using logistic regression analysis to determine independent significant factors for grade B/C POPF after PD. $P < 0.05$ was considered significant.

RESULTS

Patient Demographic and Baseline Characteristics Including Surgical Details

Baseline and operative characteristics of the 129 patients enrolled in the study are shown in Table 1. Most variables did not differ significantly between the 2 groups. However, compared with group B (n = 78), in group A (n = 51), the operation time was significantly longer ($P = 0.0086$), and external pancreatic stenting and bile duct stenting were more frequently performed ($P < 0.0001$).

Postoperative Complications

The postoperative course was complicated in 47% of the 129 patients. As shown in Table 2, there were no differences in the frequency of overall complications, septic complications, reoperation, and in-hospital death between the 2 groups. Among the listed complications, although the frequency of overall POPF was significantly higher in group B compared with group A patients (group A: 27% vs group B: 44%; $P = 0.0004$), there was no difference in the incidence of grade B/C of POPF (group A; 5.9% vs group B; 14.1%). Most POPF was classified as grade A (group A: 57%, group B: 68%) that was not clinically relevant.

TABLE 1. Patient Demographics and Baseline Characteristics

Parameters	Group A (n = 51)	Group B (n = 78)	*P*
Pancreatic duct diameter (≥3 mm:<3 mm)	35 (69):16 (31)	42 (54):36 (46)	NS
Pancreatic duct drainage (+:−)	16:35	0:78	<0.0001
Bile duct drainage (+:−)	13:38	0:78	<0.0001
Age, y	68 (51–84)	66 (36–90)	NS
Male-female ratio	33:18	51:27	NS
Disease (P:B:A)	29:9:13	46:13:19	NS
Benign-malignant ratio	4:47	13:65	NS
Total bilirubin, mg/dL	0.7 (0.3–4.7)	0.7 (0.2–3.6)	NS
AST, U/L	24 (12–77)	25 (13–236)	NS
Amylase, U/L	70 (11–473)	78 (17–300)	NS
Albumin, g/dL	3.7 (2.3–4.5)	3.9 (1.9–4.8)	NS
WBC, $\times 10^2$/mL	50 (31–98)	52 (24–124)	NS
Hb, g/dL	11.6 (8.3–14.1)	11.5 (7.7–15.8)	NS
Comorbid disease (−:+)	19:32	24:54	NS
DM (−:+)	32:19	53:25	NS
Jaundice (−:+)	18:33	32:46	NS
CRT (+:−)	7:44	5:73	NS
Type of operation (PD:PpPD)	33:18	42:36	NS
Operation time, min	523 (355–795)	468 (275–714)	0.0086
Blood loss, mL	1140 (212–6420)	952 (272–5238)	NS
Transfusion (allo:auto:none)	16:30:5	22:49:7	NS
Resection of other organs (+:−)	7:44	19:59	NS
Day of drain removal, POD	7 (4–30)	4 (3–50)	<0.0001
In-hospital stay, POD	24 (11–73)	13 (8–101)	<0.0001

Table shows median value (range) or number of patients (%).

NS indicates not statistically significant; P:B:A, pancreatic disease–biliary disease–ampullary disease; AST, aspartate aminotransferase; WBC, white blood cell count; Hb, hemoglobin; DM, diabetes mellitus; CRT, preoperative chemoradiation therapy; allo, allogenic blood transfusion; auto, autologous blood transfusion; none, no transfusion.

The leakage of PJ, as shown radiologically, was found in only 1 patient in group B. As shown in Table 2, there were no differences in the incidences of other complications. One patient (2%) in group A died at POD 31 after laparotomy because of the development of intestinal necrosis due to sudden onset of superior mesenteric arterial thrombosis. Two patients in group B required relaparotomy because of leakage of colonic anastomosis (n = 1) and intra-abdominal abscess after intractable POPF (n = 1). In group B patients, there were 3 in-hospital death caused by pneumonia (n = 2) and liver failure after leakage of colonic anastomosis. No bleeding complications or POPF-related mortality were reported in this study. The median length of postoperative in-hospital stay was significantly shorter in group B compared with group A: 13 days (range, 11–73 days) vs 24 days (range, 8–101 days), respectively ($P < 0.0001$). In more details, the length of in-hospital stay was (group B vs group A) 64% vs14% (in-hospital of <14 days), 19% vs 55% (15–29 days), and 17% vs 31% (>29 days).

Identification of Risk Factors for Grade B/C POPF

Multivariate logistic regression analyses were used to identify the risk factors associated with grade B/C POPF (Table 3). These risk factors were extracted from the results of univariate analysis for grade B/C POPF. A pancreatic duct with a diameter of less than 3 mm was the only independent risk factor for grade B/C POPF in this study.

TABLE 2. Comparison of Postoperative Complications

Parameters	Group A (n = 51)	Group B (n = 78)	*P*
Overall complications	20/51 (39%)	40/78 (51%)	NS
Septic complications	10/51 (20%)	9/78 (12%)	NS
Reoperation	1/51 (2.0%)	2/78 (2.5%)	NS
In-hospital death	1/51 (2.0%)	3/78 (3.8%)	NS
Pancreatic fistula	7/51 (14%)	34/78 (44%)	0.0004
Grade B/C	3/51 (5.9%)	11/78 (14%)	NS
DGE	3/51 (6%)	6/78 (8%)	NS
Grade A/B/C	0/1/2	3/1/2	NS
Drain infection	3/51 (5.8%)	6/78 (8%)	NS
Abdominal abscess	2/51 (3.9%)	6/78 (8%)	NS
Hemorrhage	0/51 (0%)	0/78 (0%)	NS
Wound dehiscence	10/51 (20%)	12/78 (15%)	NS
Pneumonia	1/51 (2.0%)	3/78 (3.8%)	NS
Bile leakage	1/51 (2.0%)	0/78 (0.0%)	NS
Marginal ulcer	1/51 (2.0%)	0/78 (0.0%)	NS
Peritoneal/pleural effusion	6/51 (12%)	2/78 (3%)	NS
Liver dysfunction	4/51 (7.8%)	6/78 (7.7%)	NS

Figure represents number of patients (%).

NS indicates not statistically significant; DGE, delayed gastric emptying; fluid collection, pleural effusion and/or ascites.

TABLE 3. Logistic Regression Analysis Using Perioperative Parameters for POPF (Grade B/C)

Category	Risk Factors	*P*	Relative Risk	95% CI
POPF (grade B/C)	P-duct >3 mm	—	1	
	P-duct <3 mm	0.0098	6.391	1.564–26.121

This table shows the most relevant factors in each category by multivariate analysis. The risk factor used for multivariate analysis was abstracted from the results of univariate analyses.

CI indicates confidence interval; P-duct, diameter of pancreatic duct.

Comparison of Postoperative Complications Between the 2 Subgroups in Patients With a Pancreatic Duct With a Diameter of Less Than 3 mm

In groups A and B, 31% (16/51) and 46% (36/78) of patients, respectively, had a pancreatic duct of less than 3 mm in diameter. Regarding the patients' background, there was no difference between the 2 groups (data were not published). Although there was a tendency for a higher frequency of overall POPF in group B versus group A, this did not reach statistical significance. As shown in Table 4, there were no differences between the 2 subgroups in the incidences of grade B/C POPF, delayed gastric emptying, intra-abdominal abscess formation, and other postoperative complications. In comparison of grade B/C POPF rate of 2 groups in patients with a pancreatic duct with a diameter of more than 3 mm, no significant difference was found (data not shown).

DISCUSSION

After the introduction of PD by Kausch[18] and Whipple et al,[19] the mortality rate after PD was approximately 20% in the 1970s. However, in more recent decades, morbidity and mortality rates have decreased because of improvements in perioperative management and preoperative patient selection. The development of POPF often results in severe complications, such as sepsis, intra-abdominal abscess and bleeding, and delayed gastric emptying. The safe reconstruction of pancreaticoenteric continuity after PD continues to be a challenge for the pancreatic surgeon. Although the mortality rates in high-volume centers have fallen in the past 10 years to less than 5%, morbidity still remains at 30% to 50% after PD.[1–7] To date, many efforts have been made to reduce the occurrence of POPF and mortality after PD, including the use of octreotide,[20] methods of pancreaticoenterostomy,[21–23] pancreatic duct stenting,[24,25] drain management,[26] and use of surgical microscopy.[27]

Previously, we reported rates of 5.5% for in-hospital mortality, 56% for postoperative complications, and 31% for septic complications in 198 patients who underwent PD.[8] Consequently, departmental guidelines to reduce postoperative morbidity after PD were developed and could lead to the standardization of perioperative management of PD and to a lower incidence of grade B/C POPF, delayed gastric emptying, and overall complications.[9] In that study, external stenting of the pancreatic duct was used in the limited number of patients with a pancreatic duct of less than 3-mm diameter and with a biliary duct of less than 10-mm diameter. Theoretically, external or internal stenting may help divert the pancreatic secretion away from the anastomosis.[24,25] However, severe complications associated with the stenting tube have been reported[11,12] and include acute pancreatitis due to subsequent occlusion or bending of the stenting tube or late anastomotic stenosis after iatrogenic injury sustained when withdrawing the external stenting tube.[11,12] Recently, Rezvani et al[13] reported that internal stent migration caused liver abscess formation, which was treated by percutaneous transhepatic interventional radiological approach. We have also experienced a very rare case in the early 1990s, when a patient died due to intractable pancreatojejunal anastomotic leakage after withdrawal of the external stenting tube. Other concerns were the occurrence of a catheter-related infection. Based on these experiences, we changed our procedures from duct-to-mucosa anastomosis using external stenting, to nonstented anastomosis.

In this study, there were no differences in grade B/C POPF and other major complications between the 2 groups. The overall incidence of POPF was significantly higher in group B than in group A, and there was a trend for a higher frequency of overall POPF in patients with small-diameter pancreatic ducts in group B, relative to group A. However, nonstented PJ did not increase the frequency of grade B/C POPF cases that were considered to be clinically important, even in patients with small-diameter pancreatic ducts. In this study, the methods used for PJ and perioperative management have been standardized. The population analyzed was relatively homogeneous as to clinical background, underlying diseases, clinical diagnosis, and type of operation; however, there was a tendency for more patients in group B to have small-diameter pancreatic ducts than in group A (46% vs 31%, respectively). Although the significantly higher rate of overall POPF in group B might be associated with relatively higher frequency of patients with small-diameter pancreatic ducts in this group, nonstented PJ might also, in part, have led to the increased rate of grade A POPF. Logistic regression analysis showed that the only risk factor for grade B/C POPF was small-diameter pancreatic ducts, as shown in Table 3. Subgroup analysis of patients with small-diameter pancreatic ducts showed that there was no difference between the 2 subgroups in the overall incidence of POPF, grade B/C POPF, or other complications.

External stenting across PJ anastomosis is widely used by surgeons[9,24,25,28] and may have the potential to drain pancreatic enzymes away from the PJ anastomosis. However, it was unclear whether nonstented PJ was a safe procedure. Roder et al[28] reported in a prospective study that the rate of pancreatic fistula in the external stenting group was decreased, relative to the nonstenting group. Nevertheless, as a proportion of the patients

TABLE 4. Comparison of Postoperative Complications in Subgroup of Patients in Groups A and B With a Pancreatic Duct With a Diameter of Less Than 3 mm

Parameters	Group A (n = 16)	Group B (n = 36)	*P*
Overall complications	8/16 (50%)	23/36 (64%)	NS
In-hospital death	0/16 (0%)	1/36 (2.8%)	NS
Pancreatic fistula	5/16 (31%)	21/36 (58%)	NS
Grade B/C	3/16 (19%)	8/36 (22%)	NS
DGE	1/16 (6.2%)	3/36 (8.3%)	NS
Grade A/B/C	0/1/0	2/0/1	NS

Figure represents number of patients (%).

NS indicates not statistically significant; DGE, delayed gastric emptying.

underwent PJ using the invagination technique, the findings were based on a heterogeneous population regarding the anastomotic technique used. In contrast, Imaizumi et al[12] retrospectively proposed that a stenting tube was unnecessary even in the normal pancreas if the duct-to-mucosa anastomosis performed was satisfactory. Recently, Poon et al[24] reported results from a prospective randomized trial in 120 patients over a 6-year period, which showed that external drainage of the pancreatic duct with a external stent reduced the leakage rate of PJ after PD. The differences between this study relative to ours were the longer study period, the longer period that the drains were left inserted, and the higher frequency of hemorrhagic complications, and in-hospital deaths due to POPF. In our study, the median POD that the drain was removed was 7 in group A and 4 in group B, which were earlier than POD 10 or more reported by Poon et al.[24] Moreover, there were no hemorrhagic complications or POPF-related mortality in this present study, which was also of a shorter duration than that reported by Poon et al[24] (4 years 4 months vs 6 years 4 months, respectively). The main limitation to our study was the small sample size and the retrospective nature of the analysis, which could have biased the outcome, although the study was conducted throughout by the same staff who all followed standard perioperative management procedures for the relative short study period. It is difficult to elucidate the reason for the difference in results, although the one thing they had in common was that they were single-center studies. To explore further the reasons for the different findings, it will be necessary to run a multicenter trial with the standardization of the anastomotic method and perioperative management across sites.

In this study, we would like to emphasize the shorter postoperative in-hospital stay in group B, relative to group A. In Japan, most patients do not leave the hospital until they have completely recovered because they do not have to pay for the total cost of hospital stay. In the patients who required removal of an external stenting tube, there was a tendency to later discharge from hospital. Therefore, it might be reasonable to assume that the abolishment of external stenting would be associated with shorter in-hospital stay.

Poon et al[24] proposed that stenting of the pancreatic duct allowed more precise placement of sutures, thus protecting the pancreatic duct from suture injury and reducing the risk of iatrogenic pancreatic duct occlusion, pancreatitis, and fistula formation. Indeed, duct-to-mucosa anastomosis with nonstenting can be difficult to perform when the pancreatic duct is not dilated and the lumen of duct is easily flattened in patients with normal pancreatic parenchyma. However, insertion of an ITA holder into the duct lumen enables excellent visualization without retaining the duct or pancreatic remnant.[14] In some cases, a stay-suture may be placed to open the lumen of the pancreatic duct; however, when the suture is pulled, there is a risk in that the suture material can cut easily into the pancreatic duct or parenchyma. Using an ITA holder can minimize incidental laceration of the pancreatic duct or parenchyma by replacing the need for a stay-suture; it can also minimize trauma by protecting the pancreatic duct from crush injuries caused by forceps. Thus, we firmly believe that duct-to-mucosa anastomosis without pancreatic duct stenting, and using the ITA holder, is a safe procedure.

In summary, this retrospective analysis showed that there were no differences in postoperative mortality and morbidity including grade B/C POPF development, between patients who underwent stented and nonstented PJ after PD. The multivariate analysis showed that the only risk factor for grade B/C POPF was a pancreatic duct diameter of less than 3 mm. In conclusion, the nonstented PJ using the modified Kakita method can be safely performed and is associated with a reduced length of in-hospital stay.

REFERENCES

1. Neoptolemos JP, Russel RC, Bramhall S, et al. Low mortality following resection for pancreatic and peri-ampullary tumours in 1026 patients: UK survey of specialist pancreatic units. UK Pancreatic Cancer Group. *Br J Surg*. 1997;84:1370–1376.
2. Yeo CJ, Cameron JL, Sohn TA, et al. Six hundred fifty consecutive pancreaticoduodenectomies in the 1990s. *Ann Surg*. 1997;226:248–260.
3. Boettger TC, Junginger T. Factors influencing morbidity and mortality after pancreaticoduodenectomy: critical analysis of 221 resections. *World J Surg*. 1999;23:164–172.
4. Gouma DJ, van Geenen RCI, van Gulik TM, et al. Rates of complications and death after pancreaticoduodenectomy: risk factors ad the impact of hospital volume. *Ann Surg*. 2000;232:786–795.
5. Gouillat C, Gigot JF. Pancreatic surgical complications-the case for prophylaxis. *Gut*. 2001;49:32–39.
6. Adam U, Makowiec F, Riediger H, et al. Risk factors for complications after pancreatic head resection. *Am J Surg*. 2004;187:201–208.
7. Schmidt CM, Powell ES, Yiannoutsos CT, et al. Pancreaticoduodenectomy. *Arch Surg*. 2004;139:718–725.
8. Satoi S, Takai S, Matsui Y, et al. Less morbidity after pancreaticoduodenectomy of patients with pancreatic cancer. *Pancreas*. 2006;33:45–52.
9. Satoi S, Toyokawa H, Yanagimoto H, et al. A new guideline to reduce postoperative morbidity after pancreaticoduodenectomy. *Pancreas*. 2008;37:128–133.
10. Kakita A, Yoshida M, Takahashi T. History of pancreaticojejunostomy in pancreaticoduodenectomy: development of more reliable anastomosis technique. *J Hepatobiliary Pancreat Surg*. 2001;8:230–237.
11. Ohwada S, Tanahashi Y, Ogawa T, et al. In situ vs ex situ pancreatic duct stents of duct-to-mucosa pancreaticojejunostomy after pancreaticoduodenectomy with Billroth I–type reconstruction. *Arch Surg*. 2002;137:1289–1293.
12. Imaizumi T, Hatori T, Tobita K, et al. Pancreaticojejunostomy using duct-to-mucosa anastomosis without a stenting tube. *J Hepatobiliary Pancreat Surg*. 2006;13:194–201.
13. Rezvani M, O'Moore PV, Pezzi CM. Late pancreaticojejunostomy stent migration and hepatic abscess after Whipple procedure. *J Surg Educ*. 2007;64:220–223.
14. Satoi S, Toyokawa H, Yanagimoto H, et al. Using an internal thoracic artery holder in pancreaticojejunostomy. *Surgery*. 2006;140:836–837.
15. American College of Chest Physicians/Society of Critical Care Medicine Consensus Conference: definitions for sepsis and organ failure and guidelines for the use of innovative therapies in sepsis. *Crit Care Med*. 1992;20:864–874.
16. Bassi C, Dervenis C, Butturini G, et al. Postoperative pancreatic fistula: an international study group (ISGPF) definition. *Surgery*. 2005;138:8–13.
17. Wente MN, Bassi C, Dervenis C, et al. Delayed gastric emptying (DGE) after pancreatic surgery: a suggested definition by the International Study Group of Pancreatic Surgery (ISGPS). *Surgery*. 2007;142:761–768.
18. Kausch W. Das Carcinoma der Papilla duodeni and seine radikale Entfernung. *Beitr Z Klin Chir*. 1912;78:439–486.
19. Whipple AO, Parsons WB, Mullins CR. Treatment of carcinoma of the ampulla of Vater. *Ann Surg*. 1935;102:763–779.
20. Yeo CJ, Cameron JL, Lillemoe KD, et al. Does prophylactic octreotide decrease the rates of pancreatic fistula and other complications after pancreaticoduodenectomy? Results of a prospective randomized placebo-controlled trial. *Ann Surg*. 2000;232:419–429.
21. Wente MN, Shrikhande SV, Mueller MW, et al. Pancreaticojejunostomy versus pancreaticogastrostomy: systematic review and meta-analysis. *Am J Surg*. 2007;193:171–183.

22. Bassi C, Falconi M, Molinari E, et al. Duct-to-mucosa versus end-to-side pancreaticojejunostomy reconstruction after pancreaticoduodenectomy: results of a prospective randomized trial. *Surgery*. 2003;134:766–771.
23. Tani M, Terasawa H, Kawai M, et al. Improvement of delayed gastric emptying in pylorus-preserving pancreaticoduodenectomy: results of a prospective, randomized, controlled trial: *Ann Surg*. 2006;243: 316–320.
24. Poon RT, Fan ST, Lo CM, et al. External drainage of pancreatic duct with a stent to reduce leakage rate of pancreaticojejunostomy after pancreaticoduodenectomy: a prospective randomized trial. *Ann Surg*. 2007;246:425–433.
25. Winter JM, Cameron JL, Campbell KA, et al. Does pancreatic duct stenting decrease the rate of pancreatic fistula following pancreaticoduodenectomy? Results of a prospective randomized trial. *J Gastrointest Surg*. 2006;10:1280–1290.
26. Kawai M, Tani M, Terasawa H, et al. Early removal of prophylactic drains reduces the risk of intra-abdominal infections in patients with pancreatic head resection: prospective study for 104 consecutive patients. *Ann Surg*. 2006;244:1–7.
27. Wada K, Traverso LW. Pancreatic anastomotic leak after the Whipple procedure is reduced using the surgical microscope. *Surgery*. 2006; 139(6):735–742.
28. Roder JD, Stein HJ, Bottcher KA, et al. Stented versus nonstented pancreaticojejunostomy after pancreatoduodenectomy: a prospective study. *Ann Surg*. 1999;229:41–48.

BioSystems 99 (2010) 70–78

Contents lists available at ScienceDirect

BioSystems

journal homepage: www.elsevier.com/locate/biosystems

Reproducibility and usability of chronic virus infection model using agent-based simulation; comparing with a mathematical model

Jun Itakura [a,*], Masayuki Kurosaki [a], Yoshie Itakura [a], Sinya Maekawa [b], Yasuhiro Asahina [a], Namiki Izumi [a], Nobuyuki Enomoto [b]

[a] Division of Gastroenterology and Hepatology, Musashino Red Cross Hospital, 1-26-1 Kyonan-cho, Musashino-shi, Tokyo 180-8610, Japan

[b] First Department of Internal Medicine, Faculty of Medicine, University of Yamanashi, 1110, Shimogatou, Chuou-shi, Yamanashi 409-3898, Japan

ARTICLE INFO

Article history:
Received 30 June 2009
Received in revised form 27 August 2009
Accepted 6 September 2009

Keywords:
Agent-based model
Virus infectious disease

ABSTRACT

We created agent-based models that visually simulate conditions of chronic viral infections using two software. The results from two models were consistent, when they have same parameters during the actual simulation. The simulation results comprise a transient phase and an equilibrium phase, and unlike the mathematical model, virus count transit smoothly to the equilibrium phase without overshooting which correlates with actual biology in vivo of certain viruses. We investigated the effects caused by varying all the parameters included in concept; increasing virus lifespan, uninfected cell lifespan, uninfected cell regeneration rate, virus production count from infected cells, and infection rate had positive effects to the virus count during the equilibrium period, whereas increasing the latent period, the lifespan-shortening ratio for infected cells, and the cell cycle speed had negative effects. Virus count at the start did not influence the equilibrium conditions, but it influenced the infection development rate. The space size had no intrinsic effect on the equilibrium period, but virus count maximized when the virus moving speed was twice the space size. These agent-based simulation models reproducibly provide a visual representation of the disease, and enable a simulation that encompasses parameters those are difficult to account for in a mathematical model.

1. Introduction

All viruses need hosts as a basis for their life. When a virus enters the host body, it invades cells and uses both its own enzymes and those of the host cells to replicate. Host cells infected by viruses launch a self-defense system known as the innate immune system (See and Wark, 2008; Naniche, 2009), which inhibits viral replication and uses the human leukocyte antigen system and cytokines to elicit an immune response. Immune cells that have received signals from host cells activate other immune cells, neutralize viruses in the serum by means of antibodies, and prevent the virus from replicating and proliferating by destroying or curing host cells. Viral infection is a disorder based on the interactions between viruses and cells.

The power relationship between these agents changes along with the progression of the disease. In the very early stages of infection, as the host defense mechanisms are immature, the virus has the ability to overwhelm the host cells, actively replicate, and proliferate. Subsequently, as the capacity of the immune system improves, the speed of viral proliferation drops and the virus count reaches a peak. Infected host cells begin to be disrupted by the immune system or virus particles, and symptoms appear as a result. If the immune system is stronger than the virus, then the viral counts decline, and, in transient viral disorders, the virus is finally eliminated and the host recovers. In chronic viral disorders, however, the power relationship between the virus and host cells reaches equilibrium, and a long-term power balance is maintained with the virus count reaching a plateau.

Mathematical models have been proposed to study the dynamics of such viral disorders, and are regarded as being of value in understanding this phenomenon (Ho et al., 1995; Nowak et al., 1996; Neumann et al., 1998). However, these models are difficult to understand for clinicians, and their applicability is somewhat limited in everyday practice. In clinical research, measurements of viral dynamics in patients for short duration have been made for human

Abbreviations: HIV, human immunodeficiency virus; HBV, hepatitis B virus; HCV, hepatitis C virus.

* Corresponding author. Tel.: +81 422 32 3111; fax: +81 422 32 9551.
E-mail address: jitakura@musashino.jrc.or.jp (J. Itakura).

0303-2647/$ – see front matter © 2009 Elsevier Ireland Ltd. All rights reserved.
doi:10.1016/j.biosystems.2009.09.001

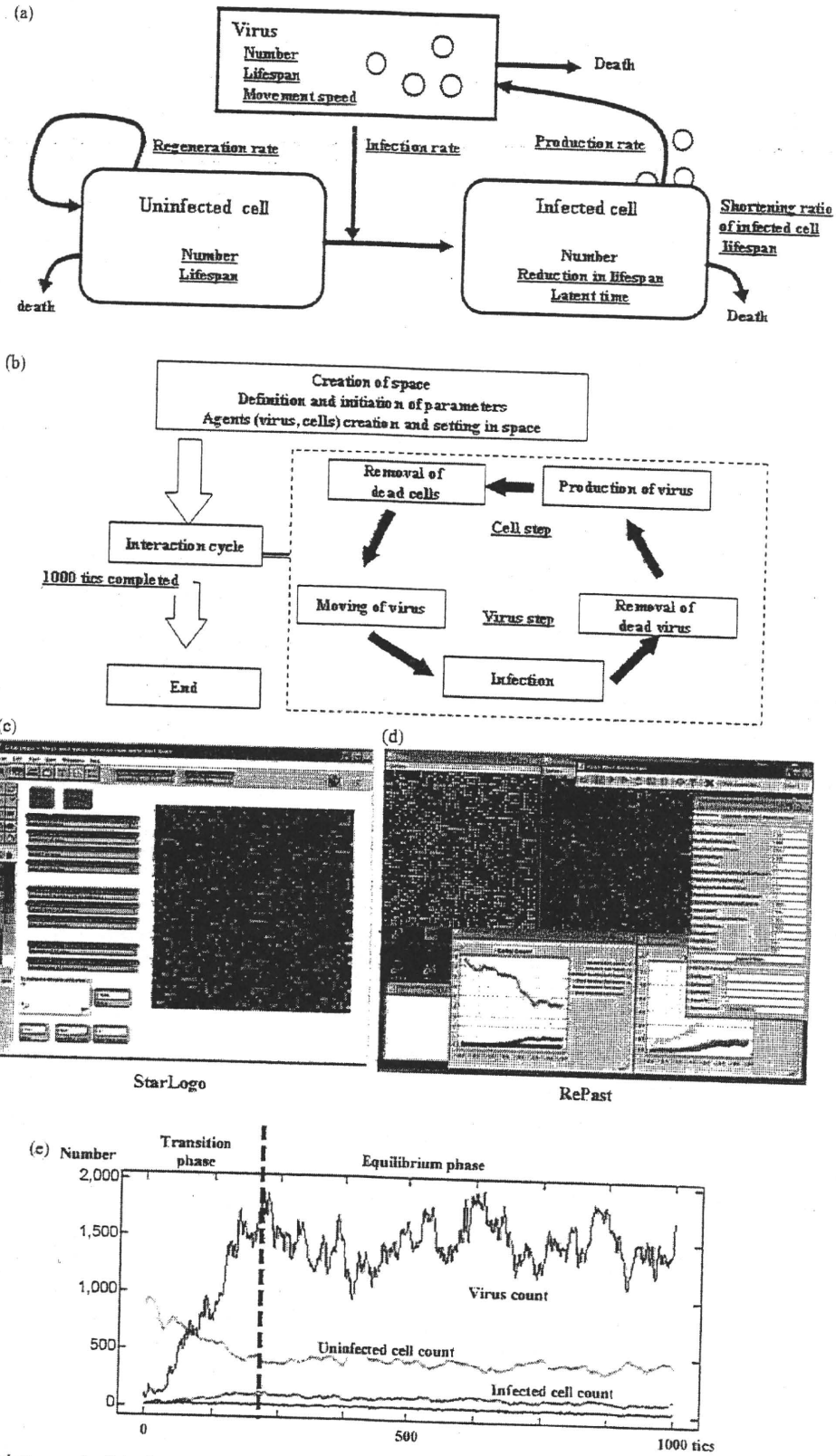

Fig. 1. Simulation design and an example of simulation results. (a) Model concept. Viruses, uninfected cells, and infected cells were treated as agents, and parameters were set for each of these and for interactions between agents (underlined). (b) Flowchart of the program. After preparing the simulation, we entered the interaction cycle, in which virus steps (such as movement) and cell steps were repeated. One cycle was counted as 1 tic, and the simulation concluded after 1000 tics. (c and d) Simulation screen using (c) StarLogo and (d) RePast. Yellow circles are viruses, green squares are uninfected cells, and orange and red indicate infected cells, with orange indicating the latent period. In StarLogo, all the agents are shown on the same screen, but in RePast, viruses and cells are shown in separate windows. (e) Example of a simulation chart in StarLogo. After the start of simulation the virus count and infected cell count increase while the uninfected cell count decreases, with equilibrium state reached after a certain number of tics.

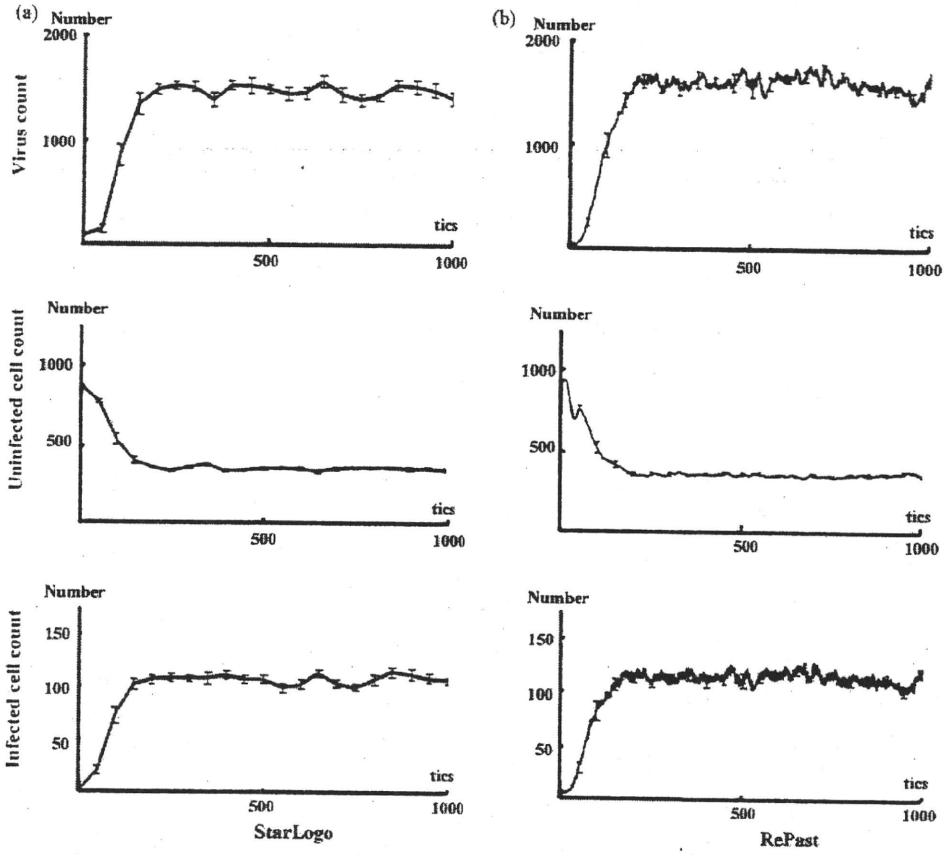

Fig. 2. Comparison of simulation results in (a) StarLogo and (b) RePast. The results were consistent when the parameters were made consistent. (Virus count [average ± SD]: StarLogo 1458.03 ± 173.1, RePast 1462.71 ± 178.8, $p = 0.94$. Uninfected cell count: 364.24 ± 30.4, 368.11 ± 33.4, $p = 0.83$. Infected cell count: 105.73 ± 13.0, 107.74 ± 13.0, $p = 0.24$. Unpaired Student's *t*-test.) Parameter values were set as follows: initial virus count, 100; uninfected cell count, 880; infected cell count, 0; virus speed of movement, 5 grids/tic; infection rate, 10%; uninfected cell regeneration rate, 1%; latent period, 3 tics; and virus reproduction rate, 5/cells/tic. The following parameter settings were taken from actual measurements: virus lifespan, 4.5 tics; uninfected cell lifespan, 49.8 tics; and infected cell lifespan, 6.7 tics.

immunodeficiency virus (HIV) (Ho et al., 1995), hepatitis B virus (HBV) (Nowak et al., 1996) and hepatitis C virus (HCV) (Neumann et al., 1998), and research is also underway on a range of models based on animal experiments and cell culture systems. As chronic viral disorders persist over long periods of time complete follow-up of viral dynamics is difficult. Furthermore, limitations of items that can be measured, such as the difficulty of measuring whole numbers of host cells, make it extremely difficult to investigate their consistency in mathematical models.

The recent ascend of dynamic-models owes much to advances in computers. Computer performance has improved markedly in recent years, not only in terms of their calculating capacity but also with regard to image displays, and models that offer a visual representation of viral disorders are now being reported (Gilbert and Bankes, 2002; Duca et al., 2007; Shapiro et al., 2008; Castiglione et al., 2007). One advantage of such visual models is that by providing a visual representation, they make understanding the disease status easy. Another benefit is that they enable parameters to be identified that are hidden as background noise in mathematical models. However, these models have some problems; it is difficult to prove the reproducibility of the simulation results derived from different languages or libraries, difficult to prove the validity of the model's concepts, and difficult to prove that the simulation results accurately reflect the reality. In this study, we created agent-based computer models that visually simulate the conditions of chronic viral infections using two software. The reproducibility of two agent-based computer models and the differences between agent-based models and the mathematical model were analyzed. This agent-based model enabled us to investigate how each parameter included in the concept affects the conditions of chronic viral infections.

2. Methods

2.1. Selection of Software

In this study, we used two different types of softwares: StarLogo version 2.0 (http://education.mit.edu/starlogo/) supplied by MIT Media Laboratory and Recursive Porous Agent Simulation Toolkit (RePast-3.0, http://repast.sourceforge.net/) supplied by the Argonne National Laboratory. StarLogo uses Logo, one of the simplest programming languages, and has a fixed graphical user interface. RePast is a library that uses Java, another programming language, which also has a fixed graphical user interface.

Logo is an assembly language, and StarLogo carries out processing sequentially. Java is an object-oriented language, and RePast has a faster processing speed than StarLogo. In addition, StarLogo has a number of stipulations to simplify simulations, such as parameters can only be set up to five decimal places and the simulation space is also fixed as 51 × 51 square grids. RePast, on the other hand, has fewer such restrictions. Thus, it offers a higher degree of freedom in program settings than StarLogo. Taking simulation space as an example, in spite of the restrictions imposed by the underlying operating system's image display system, any number of grids can be set and a hexagonal grid could also be chosen rather than a square one. However, users must stipulate and set all parameters themselves. This means that they must first declare the shape of the grid and the number of grids they will use to fill the simulation space. Java is also more difficult to learn than Logo, and debugging and correcting the program is also more difficult. Thus, it is difficult to judge whether or not the results agree with the planned simulation.

In effect, these two different types of softwares are polar opposites. It is simple to start a simulation in StarLogo, but producing results takes time and it is difficult to carry out more complex simulations. In RePast it is difficult to compose the program and judge whether or not the planned study has actually been achieved, but the

simulation itself takes only a short time to complete and there are lesser restrictions in the construction of a simulation model.

2.2. Concept for Modeling

We applied the basic virus–host interaction mathematical model to the agent-based simulation system with slight modifications. The mathematical model was used to describe the dynamics of HIV (Ho et al., 1995), HBV (Nowak et al., 1996), and HCV (Neumann et al., 1998) and the only agents involved were host cells and viruses, without the inclusion of immune cells. The effects of the immune system are expressed by varying parameters such as lifespan of host cells and viruses.

Fig. 1a illustrates the study concept. Viruses have the ability to infect healthy host cells (uninfected cells) and the infected cells produce new viruses. Both cells and viruses have definite lifespans, and the lifespan of infected cells is usually shorter than that of uninfected cells. Uninfected cells automatically regenerate within the space, whereas infected cells only arise due to infection of uninfected cells. Viruses also lack the ability to regenerate themselves and are only produced from infected cells.

2.3. Parameter Settings

In the present study, as the StarLogo settings are circumscribed, we limited the simulation space to 51 × 51 square grids. However, we made an exception here while investigating the effects of size of space on the simulation results. The numbers of viruses, uninfected cells, and infected cells could only be set before the start of the simulation. As described in the later, our simulation ran in cycles, with 1 cycle defined as 1 tic.

In mathematical simulation models, the death rate is required as a parameter. However, in our program we set lifespans for viruses and uninfected cells. These lifespans were not uniform, but were set to have a deviation of about 10%. The lifespan of cells was shortened by infection with ratio decided beforehand.

The infection ratio was meaningful only when an infected cell and a virus coincidentally occupied the same grid, and this was used to calculate the probability of the infection occurring in that situation. The virus production rate was set as the number of viruses produced by an infected cell during 1 tic. Infected cells could be set as a parameter indicating the latent period between the time of virus infection and the time of virus replication.

In order to emulate the tissue repair capacity, we set uninfected cell regeneration rate such that grids without any cells had a specified probability of producing uninfected cells on top of themselves. As a result, the more the cell count declined within a space the more regenerated uninfected cells were produced, whereas the number of regenerated cells declined as cell count increased.

The number of grids through which a virus could move in 1 tic was set as the speed of movement, and the direction of movement was set within a range of 90° toward the top of the simulation space. The program used a circulatory method of movement; when a virus arrived at the top of the space, it was translocated to the bottom, and moved again toward the top. Cells were fixed on the grid.

2.4. Simulation Flowchart

Fig. 1b shows a flowchart of the program. First, the simulation space was produced, after which each parameter was defined and the initial settings were made. Next the agents – viruses and uninfected and infected cells – were produced. The simulation cycle was as follows. Viruses moved to a new grid, and if an uninfected cell was present, this was infected with a probability based on the infection rate. The lifespan of the virus decreased, and viruses that had completed their lifespan and those that had caused an infection were removed from the space. Infected cells produced new viruses, the lifespans of both uninfected and infected cells decreased. Then, cells that had completed their lifespan were eliminated and a new cycle began. The program was set such that the simulation ended after this cycle had repeated 1000 times. This meant that one simulation was complete after 1000 tics.

2.5. Data Collection

The RePast model was programmed such that data for each tic was saved automatically as a text file at the end of the simulation. This text file could be opened by a database software. The StarLogo model was programmed to stop the simulation and collect data after every 50 tics.

2.6. Mathematical Model

In order to compare the results of this agent-based simulation, we used a viral infection mathematical model, which we improved as follows.

$$\frac{dT}{dt} = s[2601 - (T+I)] - dT - bVT \quad (1)$$

$$\frac{dI}{dt} = bVT - dI \quad (2)$$

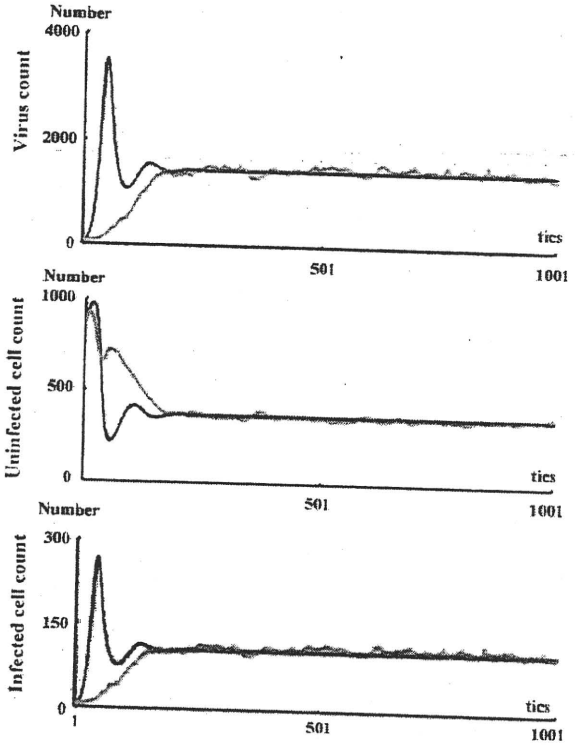

Fig. 3. Comparison of results of agent-based simulation and mathematical simulation. Both sets of results were consistent for the equilibrium phase, but differed in the shift in transition phase. Black line: mathematical model; grey line: results of simulation in RePast. Parameter values were set as follows: initial virus count, 100; uninfected cell count, 880; infected cell count, 0; virus speed of movement, 5 grids/tic; infection rate, 10%; uninfected cell regeneration rate, 1%; latent period, 3 tics; virus reproduction rate, 5/cells/tic; virus lifespan, 10 tics; uninfected cell lifespan, 50 tics; and cell lifespan-shortening ratio as a result of infection, 69%.

$$\frac{dV}{dt} = pI - cV \quad (3)$$

where, T is the uninfected cell count, I is the infected cell count, and V is the virus count. Uninfected cells are supplied to the space with a probability $s[2601 - (T+I)]$, as the number of grids in this agent-based simulation model was 2601 (51 × 51). The death rate of uninfected cells is d, the death rate of infected cells is δ, and the death rate of viruses is c. The infection rate is indicated by β. Viruses are released from infected cells at a probability p.

2.7. Statistical Analysis

Statistical analyses were performed by statistical tests using the program StatView 5.0 (SAS Institute Inc.). All tests of significance were two-tailed, with p values of <0.05 considered to be significant.

3. Results

3.1. Reproducibility of Chronic Viral Infection Disease Models Using Agent-based Simulation Methods

We constructed the chronic viral infection model with StarLogo library. Fig. 1c shows the simulation screen, and Fig. 1e shows one sample result. Immediately after the start of the simulation, the virus count temporarily dropped in accordance with the onset of an infection. Subsequently, the virus count started to increase with an increase in the infected cells and a decrease in the uninfected cells. After a certain number of tics (around 300 in this example), although the virus count, infected cell count, and uninfected cell count had some fluctuation, an equilibrium state was reached. We use the following descriptive terms in this paper: the transient phase is the period during which virus growth peaks, and the equilibrium phase is the period during which an equilibrium state is

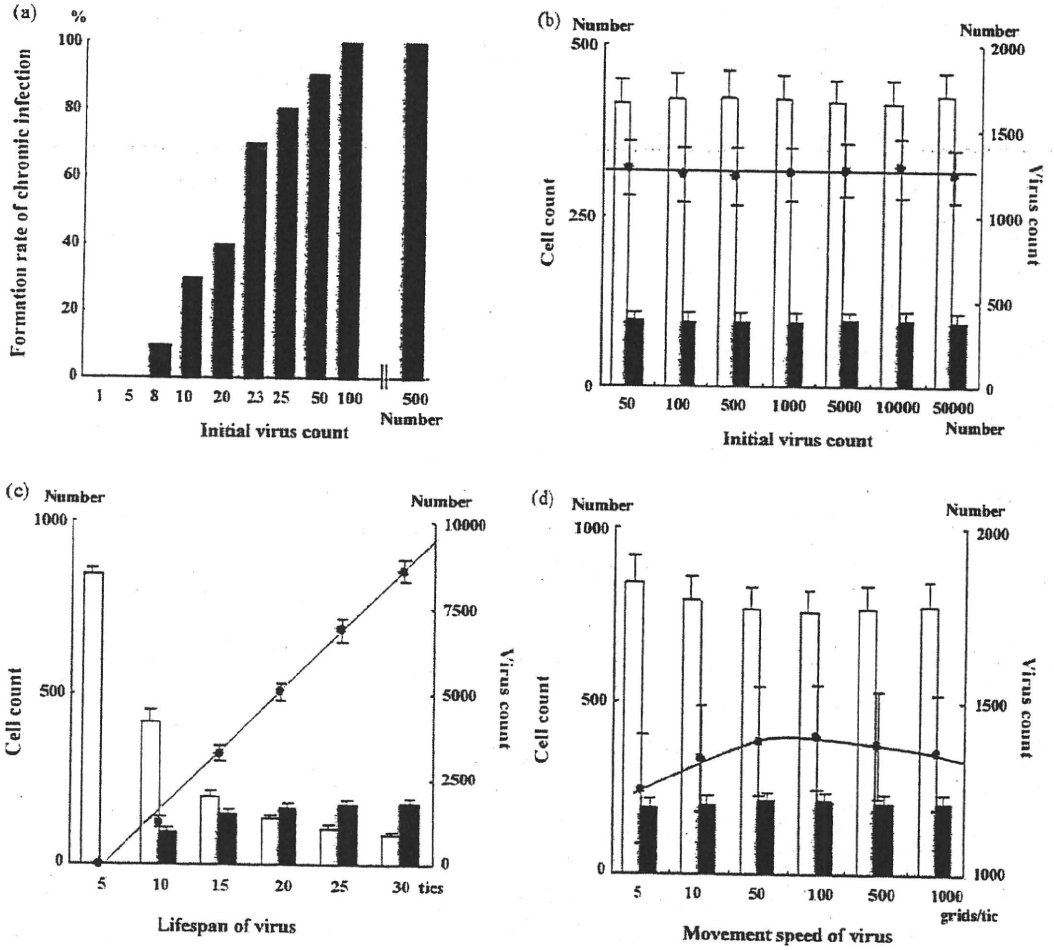

Fig. 4. Effects of changes in viral parameters. (a) The higher the initial virus count, the greater is the increase in the rate of formation of chronic infection, but (b) there was no effect on the conditions in the equilibrium phase. (c) Extending the virus lifespan increased the virus count. (d) Increasing the speed of virus movement to 100 grids/tic increased the virus count, but increasing it to 500 grids/tic had the opposite effect, with a slight declining trend. (a) Black bars: number of infections produced; (b–d) black circles: virus count; line: virus count approximation curve; white bars: uninfected cell count; black bars: infected cell count.

established. When the simulation was performed multiple times, the features described above were maintained, and the average values for virus, infected cell, and uninfected cell counts during the equilibrium state were all consistent.

Fig. 1d shows the simulation screen of the RePast. When we attempted setting all the initial parameters to the same values as those in the StarLogo, the results were not consistent. When we recalculated the parameters from the simulation results, in RePast, the parameters were largely maintained at the levels of the settings, but in StarLogo, the lifespans of both cell types became shorter than the settings while the simulation was in progress. We made the results of both simulations consistent by using the same parameters during the actual simulation (Fig. 2a and b).

3.2. Comparison Between Agent-based Simulation Models and Mathematical Simulation Model

We investigated whether the results of a chronic viral infection disease model produced by RePast would be consistent with the results of a mathematical model. For the mathematical model, we carried out an approximate integration using a four-dimensional Runge–Kutta method to ensure that the uninfected cell count and infected cell count would be in the same class. Parameters were always fixed as constant between simulations. The simulation results were consistent for the equilibrium phase, but transitions in virus count during the transient phase varied, with a shift to equilibrium state following two overshoots in the mathematical model, but a monotonic increase following a logistic curve in the agent-based model (Fig. 3). In the mathematical model, when the equilibrium condition was calculated with $dT/dt = dI/dt = dV/dt = 0$, the equilibrium-phase virus count, uninfected cell count, and infected cell count were very similar to those of the agent-based model (virus count: mathematical model 371.8/space, agent-based model 371.1 ± 32.4/space [average ± SD]; uninfected cell count: mathematical model 1605/space, agent-based model 1454 ± 194/space; infected cell count: mathematical model 115.9/space, agent-based model 108.3 ± 14.2/space).

3.3. Usability of the Models; Effect of Changing Parameters

We investigated the changes in the equilibrium phase brought about by changing each parameter. All the investigations below were carried out by using RePast, and we used the average values from ten simulations.

3.4. Viral Parameters

The lower the virus counts at the beginning of the simulation, the lower the probability of a chronic infection (Fig. 4a). However, the initial virus count did not have any effect on the equilibrium

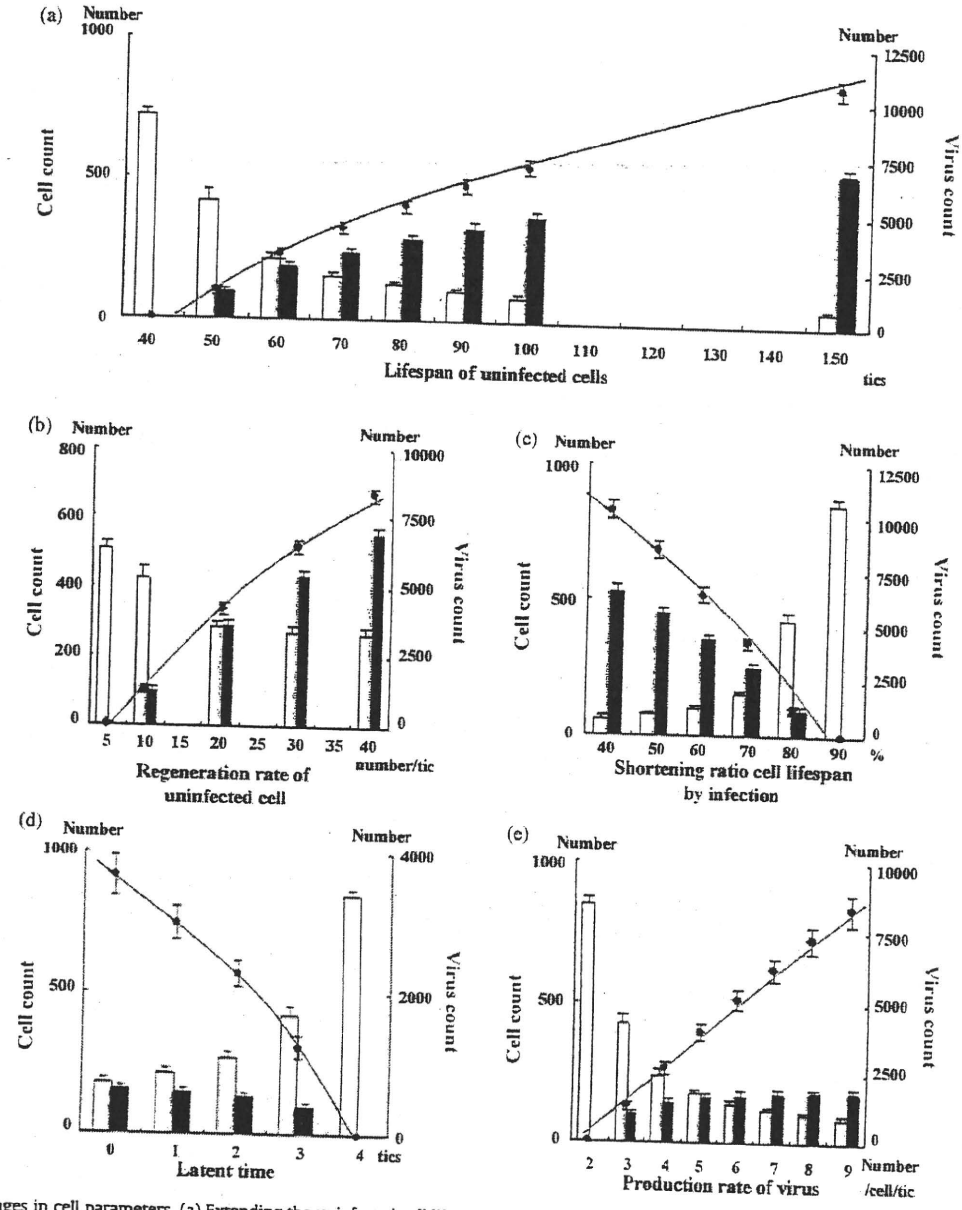

Fig. 5. Effects of changes in cell parameters. (a) Extending the uninfected cell lifespan and (b) increasing the uninfected cell regeneration rate increased the virus count. (c) Raising the lifespan-shortening ratio as a result of infection shortened the lifespan of infected cells, thereby decreasing the virus count. (d) Extending the latent period shortened the period of virus production from infected cells, thereby decreasing the virus count. (e) Increasing the virus production count resulted in a linear increase in equilibrium-phase virus count. Black circles: virus count; line: virus count approximation curve; white bars: uninfected cell count; black bars: infected cell count.

phase itself (Fig. 4b). Extending the lifespan of viruses resulted in a linear increase in equilibrium-phase virus count (Fig. 4c). Although the infected cell count increased, the rate of increase gradually declined. Changing the speed of viral movement resulted in the equilibrium-phase virus count to eventually decline after 100 grids/tic was reached, allowing movement over an area twice the size of the simulation space (Fig. 4d).

3.5. Uninfected Cell Parameters

Extending the lifespan of uninfected cells led to an increased virus count during the equilibrium phase (Fig. 5a). Increasing the uninfected cell regeneration rate also contributed to increased equilibrium-phase virus count (Fig. 5b). In both the cases, the increases in virus count and infected cell count were not linear, but showed a tendency for the rate of increase to decline gradually.

3.6. Infected Cell Parameters

We carried out an investigation of the effects of variation in the lifespan-shortening ratio on the virus count on the assumption that cell lifespan is shortened by infection. When this ratio was increased, the virus count decreased (Fig. 5c). An extended latent period was also related to a decreased virus count (Fig. 5d). However, the virus production from infected cells led to a linear increase in the virus count (Fig. 5e).

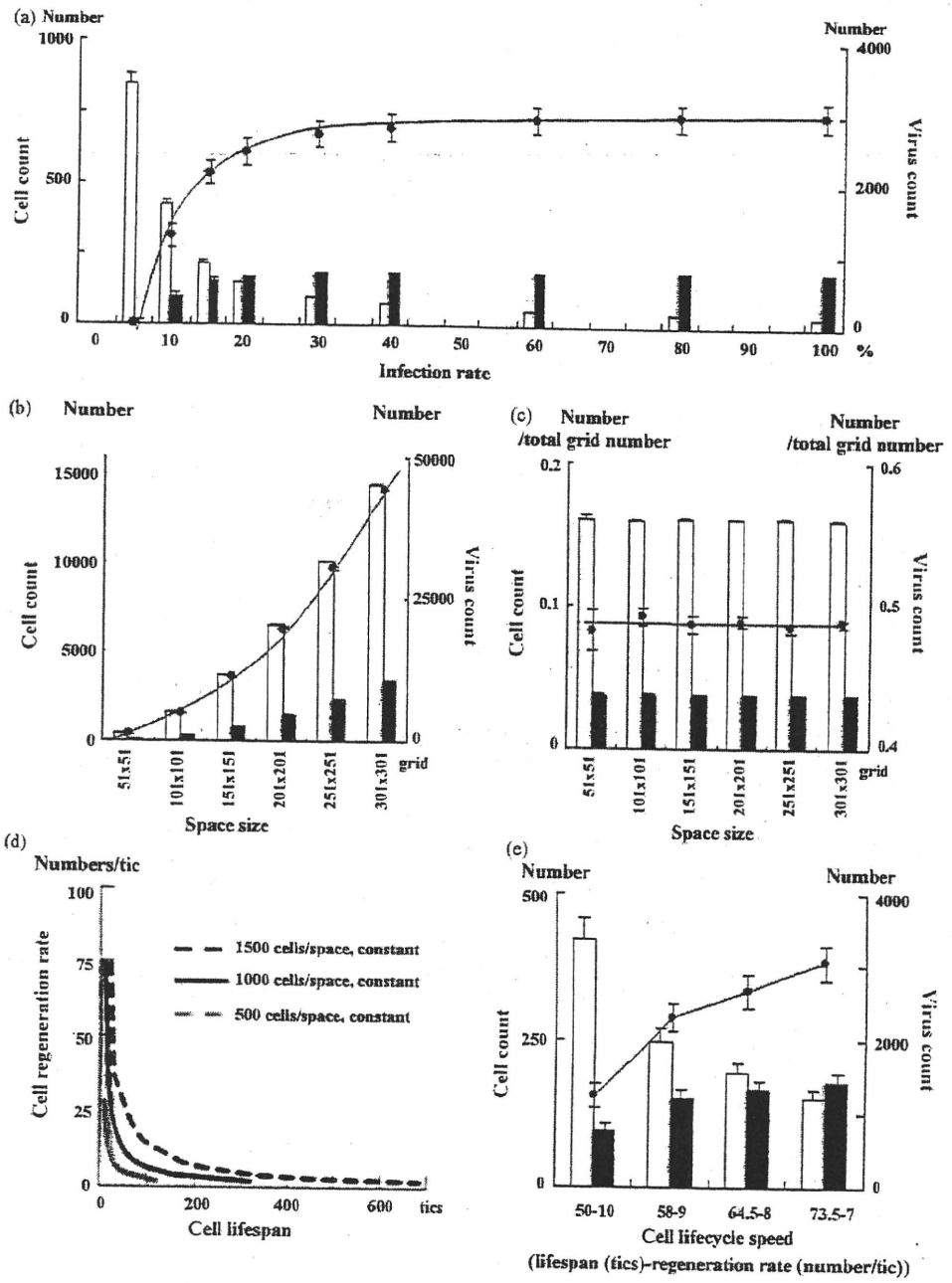

Fig. 6. (a) Increasing the infection rate increased the virus count in equilibrium periods, but the virus count did not change at infection rates of 30% or more. (b) The size of the simulation space increased not only virus count but also the cell count; however, (c) when virus and cell counts were divided by the total number of grids in the space, they were constant for all space sizes. (d) Changing the lifespan and regeneration rate of uninfected cells in opposite directions at the same time makes it possible to change only the cell cycle speed without altering the uninfected cell count. (e) When the cell cycle speed was reduced, the virus count increased toward the right of the graph. This may be because the effect of extending the lifespan of cells exceeds that of reducing their regeneration rate. (a–c and e) Black circles: virus count; line: virus count approximation curve; white bars: uninfected cell count; black bars: infected cell count.

3.7. Infection Rate and Space Size

Increasing the infection rate caused an increase in the virus count, but the change was minimal at an infection rate of 30% or more. The same results were seen for infected cell count, but a decrease in uninfected cell count resulted in a tendency for the infection rate to decrease by up to 60% (Fig. 6a).

The larger the space, higher the increase in both virus and cell counts (Fig. 6b). This increase was proportional to space size, however, when virus and cell counts were divided by the total number of grids in the space they were all constant (Fig. 6c).

3.8. Cell Cycle Speeds

Running a simulation with the initial virus count set to zero enables only the equilibrium condition for uninfected cells to be simulated. Changing the lifespan and regeneration rate of uninfected cells in opposite directions at the same time makes it possible

to change the cell cycle speed without altering the uninfected cell count (Fig. 6d). We used this technique to investigate how changing the cell cycle speed affected the equilibrium phase. Fig. 6e shows the results. Cell lifespan increases while the cell cycle speed declines. The equilibrium virus count increased in accordance with slower cell cycle speeds.

4. Discussion

In this study, we investigated the models using two agent-based simulation methods to program a simple virus–host chronic infection model. The same model written in two different programming language systems displayed the same results. The transient phase was unlike that seen in a mathematical simulation with no overshoot in virus count, but rather a smooth transition to the equilibrium phase. The virus count at the start of the simulation only had effect on the rate of infection development. Increases in virus lifespan, uninfected cell lifespan, uninfected cell regeneration rate, virus production count from infected cells, and infection rate all led to increased equilibrium-phase virus count. Rises in the infected cell lifespan-shortening ratio, latent period, and cell cycle speed decreased the equilibrium-phase virus count. The size of the space itself had no innate effect on the equilibrium phase, but a speed of movement of the virus that was twice the size of the space produced the maximum virus count.

Reproducibility is the basis for all scientific study, but there are many problems to prove it in computer simulations, such as programming bugs. As agent-based simulation deals with numerous agents individually, it requires vast amounts of calculations. Accumulation of very small change of values leads to large differences of results. In this study, we investigated two programs based on two programming languages to confirm the reproducibility of our simulation results in different programming languages. The results of two simulations were consistent, but in StarLogo, the lifespan parameters had a tendency to be lower than when they were set while simulations were actually in progress. This may be because the number of digits used in calculations was different between the two programs. RePast performs calculations to at least eight decimal places. In StarLogo, the library settings only enable settings to be made up to five decimal places. It is probable that these small differences accumulate during repeated calculations and are reflected in the simulation. Ultimately, we confirmed that the differences in results obtained by using different libraries and programming languages were not innate and by making the parameters consistent during simulation, consistent results were obtained.

Mathematical models using formulae for HIV therapy was published in 1994, the method has since been applied to HBV and HCV (Ho et al., 1995; Nowak et al., 1996; Neumann et al., 1998), and they were thought to be good reflections of the reality. In the mathematical model, viruses and cells are conceived as individuals in the concept itself, but both of them are perceived *en masse* when calculations are performed. However a feature of the agent-based simulation is that it deals with individual viruses and cells as separate agents. By moving each agent individually, it probes the factors influencing overall shifts from the micro viewpoint. When the space is viewed as a whole, it is possible to watch on the screen the collective movement of groups of agents. Recently, models that provide a visual representation of Epstein–Barr virus and HIV infection have been reported, both of which are useful for an instinctive and intuitive understanding (Duca et al., 2007; Shapiro et al., 2008; Castiglione et al., 2007).

In agent-based simulation model, virus count transit smoothly to the equilibrium phase. On the other hand, virus counts overshoot during transient phase in mathematical model. We think this difference is derived from technicality of different modeling. The difference in concepts between mathematical models and agent-based models is the space. The mathematical model has no space in concept, but agents move across the space in the agent-based model. In agent-based models, the densities of virus and cells change overtime especially in the transition phase because of the limited space. These changes of the densities of virus and cells lead to the dynamic change of the encounter rate of viruses and cells. The mathematical model does not make such concept of the density; the encounter rate is constant. This may be the reason for the difference between two models in the transition phase. Since no overshoot of virus counts in transient phase had been reported from in vivo studies of hepatitis C virus and simian immunodeficiency virus (Dahari et al., 2005; Nowak et al., 1997), agent-based model correlates with actual biology in vivo at least for these viruses. The increase of initial virus count at the start of simulation correlates with higher encounter rate of viruses and cells which make the linear increasing of infection forming rate. Mathematical model can only express the infection formation rate as "infected or not".

The importance of viral passing speed in the agent-based model is also explained by the "space". Although the virus actually moves through the blood stream in our body and virus could not decide their moving speeds by themselves, there is most appropriate speed for virus to meet the cells on the simulation space by the highest probability. The effect of cell cycle speed should be mentioned by another affection of the space. A fast cell cycle speed means that the lifespan of uninfected cells is short. Then fast cell cycle speed leads to the short lifespan of infected cells. A higher regeneration rate for uninfected cells results in a higher rate of infection among uninfected cells by viruses, but in situations where viruses and cells are dispersed around the space this is ineffective in increasing the infection rate, as the latter depends on the probability that they will encounter one another. As a result, the infected cell count decreases during the equilibrium phase, as does the virus count.

In this study, we confirmed the reproducibility and usability of agent-based models in expressing the interaction between viruses and cells. A feature of this simulation system is that it uses the concept of space as actual space, which means that the existence of the space becomes an additional controlling factor on the simulation results. This is a concept that is absent from mathematical models. The reality is that we have a spatial existence, and an advantage of the agent-based simulation system is the fact that it accounts for the space. Another feature of the simulation system is that it enables the condition to be perceived in visual terms, making it easy to understand. However it may be affected by computer performance and by the limitations of programming languages or the program itself, this system may offer a powerful tool for the future analysis of real virus–host interaction disease.

Conflict of interest

No conflicts of interest exist for all authors.

References

Castiglione, F., Pappalardo, F., Bernaschi, M., Motta, S., 2007. Optimization of HAART with genetic algorithms and agent-based models of HIV infection. Bioinformatics 23, 3350–3355, doi:10.1093/bioinformatics/btm408.

Dahari, H., Major, M., Zhang, X., Mihalik, K., Rice, C.M., Perelson, A.S., Feinstone, S.M., Neumann, A.U., 2005. Mathematical modeling of primary hepatitis c infection: noncytolytic clearance and early blockage of virion production. Gastroenterology 128, 1056–1066, doi:10.1053/j.gastro.2005.01.049.

Duca, K.A., Shapiro, M., Delgado-Eckert, E., Hadinoto, V., Jarrah, A.S., Laubenbacher, R., Lee, K., Luzuriaga, K., Polys, N.F., Thorley-Lawson, D.A., 2007. A virtual look at Epstein-Barr virus infection: biological interpretations. PLoS Pathog. 3, 1388–1400, doi:10.1371/journal.ppat.0030137.

Gilbert, N., Bankes, S., 2002. Platforms and methods for agent-based modelling. Proc. Natl. Acad. Sci. U.S.A. 99 (Suppl. 3), 7197–7198.

Ho, D.D., Neumann, A.U., Perelson, A.S., Chen, W., Leonard, J.M., Markowitz, M., 1995. Rapid turnover of plasma virions and CD4 lymphocytes in HIV-1 infection. Nature 373, 123–126, doi:10.1038/373123a0.

Naniche, D., 2009. Human immunology of measles virus infection. Curr. Top. Microbiol. Immunol. 330, 151–171.

Neumann, A.U., Lam, N.P., Dahari, H., Gretch, D.R., Wiley, T.E., Layden, T.J., Perelson, A.S., 1998. Hepatitis C viral dynamics in vivo and the antiviral efficacy of interferon-alpha therapy. Science 282, 103–107, doi:10.1126/science.282.5386.103.

Nowak, M.A., Bonhoeffer, S., Hill, A.M., Boehme, R., Thomas, H.C., McDade, H., 1996. Viral dynamics in hepatitis B virus infection. Proc. Natl. Acad. Sci. U.S.A. 93, 4398–4402.

Nowak, M.A., Lloyd, A.L., Vasquez, G.M., Wiltrout, T.A., Wahl, L.M., Biscofberger, N., Williams, J., Kinter, A., Fauci, A.S., Hirsch, V.M., Lifson, J.D., 1997. Viral dynamics of primary viremia and antiretroviral therapy in simian immunodeficiency virus infection. J. Virol. 71, 7518–7525.

Shapiro, M., Duca, K.A., Lee, K., Delgado-Eckert, E., Hawkins, J., Jarrah, A.S., Laubenbacher, R., Polys, N.F., Hadinoto, V., Thorley-Lawson, D.A., 2008. A virtual look at Epstein-Barr virus infection: simulation mechanism. J. Theor. Biol. 252, 633–648, doi:10.1016/j.jtbi.2008.01.032.

See, H., Wark, P., 2008. Innate immune response to viral infection of the lungs. Paediatr. Respir. Rev. 9, 243–250, doi:10.1016/j.prrv.2008.04.001.

Digestive Endoscopy (2009) **21**, 67–72

doi:10.1111/j.1443-1661.2009.00844.x

REVIEW

LAPAROSCOPIC RADIOFREQUENCY ABLATION FOR HEPATOCELLULAR CARCINOMA

YASUHIRO ASAHINA, HIROYUKI NAKANISHI AND NAMIKI IZUMI

Division of Gastroenterology and Hepatology, Musashino Red Cross Hospital, Kyonan-cho, Musashino-shi, Tokyo, Japan

Radiofrequency ablation (RFA) is one of the best curative treatments for hepatocellular carcinoma in selected patients, and this procedure can be applied either percutaneously or laparoscopically. Although the percutaneous approach is less invasive and is considered the first choice, RFA with laparoscopic guidance is highly recommended for patients with a relative contraindication for percutaneous RFA, such as lesions adjacent to the gastrointestinal tract, gallbladder, bile duct and heart. Recent advances in laparoscopic ultrasound have widened the indication for laparoscopic ablation. In the present paper, we review the indications, advantages, prognosis and safety of laparoscopic RFA for hepatocellular carcinoma.

Key words: hepatocellular carcinoma, laparoscopic ultrasonography, laparoscopy, radiofrequency ablation.

INTRODUCTION

Hepatocellular carcinoma (HCC) is one of the most frequent primary hepatic malignancies, not only in Japan, but also in the USA and Europe.[1–4] HCC is closely linked to chronic liver diseases including hepatitis B and hepatitis C.[5] Surveillance of these patients can lead to an HCC diagnosis at an early stage, when the tumor may be cured with resection, liver transplantation or local ablation.[6–8] Unlike other solid tumors, surgical resection plays a limited role in the treatment of hepatocellular carcinoma,[7,9,10] because underlying cirrhosis or multiple lesions often contraindicate surgery. Furthermore, this cancer frequently recurs, even after apparently curative resection.[11] Liver transplantation may be effective in highly selected patients,[12] but its feasibility is restricted by the shortage of donors.[13,14] Hence, several alternative non-surgical treatments to potentially cure HCC have been developed.

Radiofrequency ablation (RFA), also known as radiofrequency thermal ablation, is a recently developed thermoablative technique.[15–18] It induces temperature changes by using high-frequency alternating current applied via electrodes placed within the tissue to generate areas of coagulative necrosis and tissue desiccation.[19,20] RFA can be applied percutaneously, laparoscopically or during open surgery.

In 1997, Curley *et al.* performed a feasibility study of laparoscopic RFA on pigs demonstrating the simplicity of the procedure,[21] and favorable results were subsequently achieved in preliminary clinical experience.[22–24] The laparoscopic approach has the benefits of direct visual control of the RFA procedure, exposure and isolation of the liver from the surrounding tissue, and effective management of intraoperative bleeding.[25]

Correspondence: Namiki Izumi, Division of Gastroenterology and Hepatology, Musashino Red Cross Hospital, 1-26-1 Kyonan-cho, Musashino-shi, Tokyo 180-8610, Japan. Email: nizumi@musashino.jrc.or.jp

Received 24 October 2008; accepted 5 January 2009.

INDICATIONS FOR LAPAROSCOPIC RFA AS A CURATIVE TREATMENT

The current indications for laparoscopic RFA as a curative therapy are similar to percutaneous RFA: three or fewer tumors measuring ≤3 cm in diameter, or a solitary tumor with a major axis of ≤5 cm and liver function of Child–Pugh class A or B. Although curative ablation is possible for tumors measuring ≤2 cm in diameter, there is no clear evidence that ablation can cure hypervascular HCC >3 cm in diameter. HCC with extrahepatic metastasis, and vascular or biliary invasion should be excluded from the indication.

Similar to percutaneous RFA, the contraindications for laparoscopic RFA are jaundice, refractory ascites, and a tendency for hemorrhage (platelet count $<50 \times 10^9$/L or prothrombin activity <50%). However, RFA with laparoscopic guidance is highly recommended for patients with a relative contraindication for percutaneous RFA, such as lesions adjacent to the gastrointestinal tract, gallbladder, bile duct or heart.[26] Contraindications specific to laparoscopic RFA are the same as for generic laparoscopy and include previous abdominal surgery, cardiopulmonary disorders and severe obesity.

LAPAROSCOPIC RFA PROCEDURE

Laparoscopic RFA is usually carried out under general anesthesia. After infusing carbon dioxide gas into the peritoneal cavity to generate a pneumoperitoneum, a laparoscope is inserted through a 5–10 mm trocar depending on its diameter. A mesh-covered access port (VersaStep®; US Surgical, Norwalk, CT, USA) is recommended to avoid arterial bleeding from the abdominal wall and to avoid visceral injury. After the endoscopic examination, a laparoscopic ultrasound probe is inserted through the second trocar to screen, detect and determine the puncture point for the tumor (Fig. 1). The RF electrode is inserted under ultrasonic guidance (Fig. 1), and ablation is carried out as many times as needed. Either an expandable electrode with a thermo-controlled generator

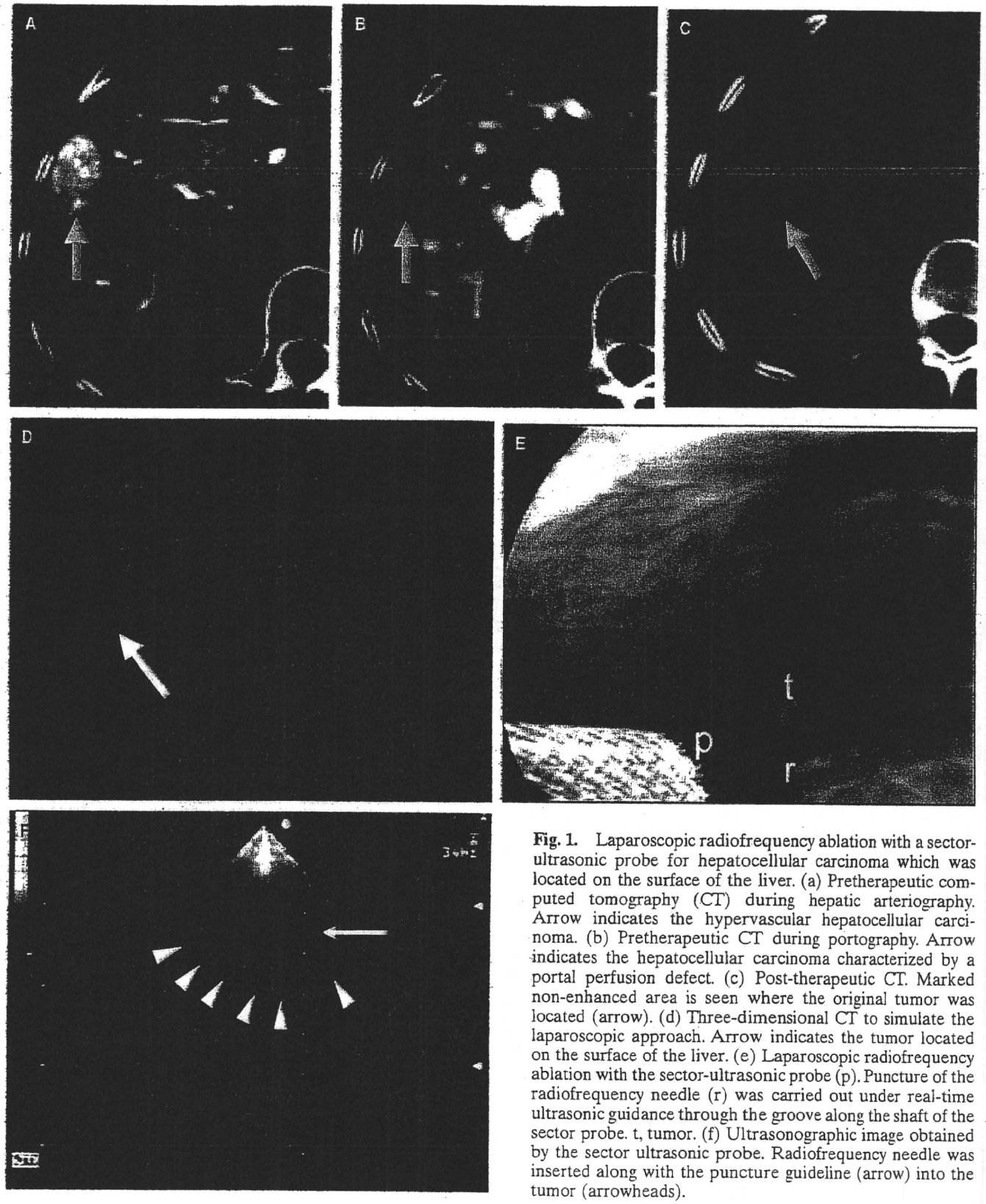

Fig. 1. Laparoscopic radiofrequency ablation with a sector-ultrasonic probe for hepatocellular carcinoma which was located on the surface of the liver. (a) Pretherapeutic computed tomography (CT) during hepatic arteriography. Arrow indicates the hypervascular hepatocellular carcinoma. (b) Pretherapeutic CT during portography. Arrow indicates the hepatocellular carcinoma characterized by a portal perfusion defect. (c) Post-therapeutic CT. Marked non-enhanced area is seen where the original tumor was located (arrow). (d) Three-dimensional CT to simulate the laparoscopic approach. Arrow indicates the tumor located on the surface of the liver. (e) Laparoscopic radiofrequency ablation with the sector-ultrasonic probe (p). Puncture of the radiofrequency needle (r) was carried out under real-time ultrasonic guidance through the groove along the shaft of the sector probe. t, tumor. (f) Ultrasonographic image obtained by the sector ultrasonic probe. Radiofrequency needle was inserted along with the puncture guideline (arrow) into the tumor (arrowheads).

system (e.g. RITA Medical Systems, Inc., Mountain View, CA, USA)[27] or an internally water-cooled electrode with an impedance-controlled generator (e.g. Cool-tip system; Radionics, Burlington, MA, USA)[28] is used. The specification of these electrodes and generators has been discussed elsewhere.[27,28]

The main difficulty, as in all laparoscopic ultrasound-guided procedures, is the insertion of the needle into the lesion, because of the presence of a double fulcrum presented by the abdominal wall and the hepatic parenchyma. Specific expertise is necessary to avoid repeated passage of the needle. To prevent tumor dissemination, the RF needle should be inserted through normal liver tissue to avoid direct puncture of the tumor. Based on our experience, an endoretractor is useful to expose the tumor and to protect against visceral injury in the event that the tumor is located on the inferior surface, which is hidden by adjacent viscera. Other techniques reported in the literature include three-dimensional computed tomography to simulate the laparoscopic strategy (Fig. 1), the use of a cutter to remove adhered mesentery,[29] or a combination of hand-assisted laparoscopic surgery[30] and liver resection.[31]

ADVANTAGES OF THE LAPAROSCOPIC APPROACH

The laparoscopic approach offers the advantages of a minimally invasive procedure including direct visual control of the RFA procedure, exposure and isolation of the liver from the surrounding tissue, and the management of intraoperative complications.[25]

The treatment of a HCC on the superior or inferior surface of the liver can potentially ablate the adjacent abdominal wall or, worse, the adjacent viscera with the possibility of major post-procedure complications and tumor seeding.[32–34] Hence, the laparoscopic approach is well indicated in superficial or extrahepatic protrusive HCC, and HCC adjacent to the gastrointestinal tract, gallbladder, bile duct or heart.[35,36] In cases of paracholecystic HCC, the laparoscopic procedure allows for a cholecystectomy and enables a direct approach through the gallbladder fossa to ablate the tumor.[24,37] The laparoscopic approach with a positive-pressure pneumoperitoneum has a distinct advantage over the percutaneous approach because liver blood flow is reduced by approximately 40%.[38]

BENEFITS OF LAPAROSCOPIC ULTRASOUND

The laparoscopic approach also offers the ability to carry out an intraoperative high-frequency ultrasound examination. Using laparoscopic ultrasound during the procedure can help identify the treatable lesion, detect new HCC lesions that were not identified by preoperative imaging,[39–44] and aid RF-needle placement for more accurate targeting.[37,45–50] Initially, laparoscopy and laparoscopic ultrasound were found to be useful for staging and detecting new HCC that could not be identified preoperatively.[39–44,48] With advances in laparoscopic ultrasonographic probes, the role of laparoscopic RFA has become particularly important in the subdiaphragmatic area where percutaneous ultrasound has limited use for detecting tumors and increases the risk for diaphragmatic thermal injury.

With advances in technology, several types of laparoscopic ultrasonographic probes have been developed. The linear scan type, which was originally designed to assist during laparoscopic cholecystectomy, has been applied to laparoscopic RFA (e.g. flexible 7.5-MHz probe, Aloka Co., Tokyo, Japan; 7.5-MHz linear array probe, Hitachi Co., Tokyo, Japan and B&K Medical, Copenhagen, Denmark). Despite its good image resolution, a linear probe requires skill and experience,[45,51–53] or the development of special navigation technology,[47–50] to precisely target a tumor for ablation. This clinical obstacle has been overcome by new types of ultrasonic probes; the sector type (Aloka Co.)[37] and the convex scan type (PVM-787LA; Toshiba Medicals, Tokyo, Japan).[46] These probes are designed to target intrahepatic tumors because they have a guiding tract on the shaft that allows the user to see an ablation needle advancing into a tumor on a real-time ultrasonographic image. This feature has widened the indication for laparoscopic ablation in cases where tumors are located beneath the surface away from the direct view of the laparoscope.

EFFICACY AND PROGNOSIS

The overall local recurrence rate of RFA using the percutaneous and laparoscopic approaches varies from 1.8 to 14%.[54–59] The local recurrence rate of laparoscopic RFA varies from 0 to 12%.[22,24,37,40,46,52,53,60–63] Many of these studies have suggested that local control of the laparoscope is an advantage during laparoscopic RFA compared with the percutaneous approach. Reported factors associated with the risk of local recurrence include an HCC with multiple lesions, size >30 mm in diameter, infiltrative type, capsular invasion, vascular invasion and an inadequate ablation margin.[60,61,63] The risk of local recurrence increases with an increase in HCC size, but the local recurrence rate differs markedly if a circumferential 5-mm safety margin can be secured. In addition, risk factors associated with distant recurrence after RFA are multiple HCC and hepatitis C viral infection.[64]

Although the short history of RFA prevents an analysis of long-term prognosis, several reports have indicated a 3-year survival rate of 40–60%.[65,66] We found no local recurrence in our series of 84 patients with HCC who underwent curative laparoscopic RFA from 1999 as an initial therapy, whereas the 1-year local recurrence rate in patients treated with percutaneous RFA ($n = 485$) was 3.9%. The cumulative survival rates at 1, 3 and 5 years in patients with laparoscopic RFA as an initial therapy were 100%, 84% and 81%, respectively ($n = 84$), which was comparable to patients with percutaneous RFA (96%, 1 year; 83%, 2 years; and 61%, 3 years, $n = 485$) (Fig. 2). Similar to percutaneous RFA, survival after laparoscopic RFA was determined by Child–Pugh class and alpha fetoprotein (AFP) levels.[65] It must be emphasized that operator skill, securing a safety margin around the tumor, accurate evaluation of the therapeutic response and an aggressive treatment all closely affect the results.

SAFETY

Safety is one of the most important issues in minimally invasive therapies such as laparoscopic RFA. The rate of major complication for laparoscopic RFA is reported to be 3.8%,[66]

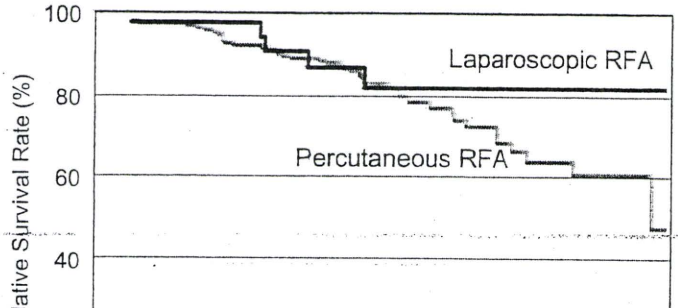

Fig. 2. Cumulative survival rate in patients with hepatocellular carcinoma who underwent laparoscopic (solid line, $n = 84$) or percutaneous (gray line, $n = 485$) radiofrequency ablation as an initial curative treatment in Musashino Red Cross Hospital from 1999.

which is lower than laparotomy,[62] transcatheter arterial chemoembolization[67] and percutaneous RFA.[68] Complications from laparoscopic RFA include liver failure, bile-duct thermal injury, liver abscess, pneumothorax, pneumonia, trocar injury involving the small bowel or gallbladder, postoperative bleeding from the mesentery, gastrointestinal bleeding, hepatic infarction, skin burns, pacemaker malfunction, congestive heart failure, hemoglobinuria and myoglobinuria.[61,62,67,69,70] Complications specific to laparoscopic RFA are pneumonia, pneumothorax, trocar injury and postoperative bleeding from the mesentery or abdominal wall. In our series of HCC patients who underwent laparoscopic RFA, 2.2% (2/92) had postoperative complications, which was comparable to the 2.0% (27/1333) observed for percutaneous RFA (Table 1).

In our experience, the use of a mesh-covered access port (VersaStep™) avoids trocar injury and bleeding from the mesentery and abdominal wall. The mandatory use of laparoscopic-ultrasound guidance during RF-needle puncture will avoid thermal injury to the intrahepatic vessels and/or bile duct and to adjacent organs such as the diaphragm, heart, gallbladder and intestine. Because patients with a history of biliopancreatic surgery have a higher rate of liver abscess formation,[66] special caution should be paid to these patients after the procedure.

CONCLUSION

Laparoscopic RFA is a safe and feasible treatment to cure an HCC tumor in selected patients. The main advantages of the laparoscopic approach are better neoplastic staging, and the ability to treat lesions for which percutaneous RFA is contraindicated or risky. The main disadvantages of this technique are the need to carry out the procedure under general anesthesia, its invasive nature compared with the percutaneous approach, and the risk of complications from the laparoscopy. Laparoscopic RFA should be considered complementary and not an alternative technique to percutaneous RFA. In order to define the indications for laparoscopic RFA, it is essential to develop considerable experience in the procedure and conduct clinical trials in comparison with other therapeutic techniques.

Table 1. Complications of laparoscopic and percutaneous radiofrequency ablation for hepatocellular carcinoma at the Musashino Red Cross Hospital

	Laparoscopic RFA $n = 92$	Percutaneous RFA $n = 1333$
Biliary fistula	0 (0%)	4 (0.30%)
Liver abscess	1 (1.1%)	4 (0.30%)
Intercostal arterial bleeding	0 (0%)	3 (0.22%)
Hemothorax	0 (0%)	2 (0.15%)
Liver infarction	0 (0%)	3 (0.22%)
Liver dysfunction	0 (0%)	2 (0.15%)
Tumor dissemination	0 (0%)	4 (0.30%)
Skin burn	0 (0%)	2 (0.15%)
Subcutaneous hematoma	1 (1.1%)	0 (0%)
Pneumothorax	0 (0%)	2 (0.15%)
Intestinal perforation	0 (0%)	1 (0.07%)
Total	2/92 (2.2%)	27/1333 (2.0%)

REFERENCES

1. El-serag HB, Mason AC. Rising incidence of hepatocellular carcinoma in the United States. *N. Engl. J. Med.* 1999; **340**: 745–50.
2. Taylor-Robinson SD, Foster GR, Arora S, Hargreaves S, Thomas HC. Increase in primary liver cancer in the UK, 1979–94. *Lancet* 1997; **350**: 1142–3.
3. Llovet JM, Burroughs A, Bruix J. Hepatocellular carcinoma. *Lancet* 2003; **362**: 1907–17.
4. Okuda K, Okuda H. Primary liver cell carcinoma. In: Mcintyre N, Benhamou JP, Bircher J, Rizzetto M, Rodes J (eds). *Oxford Textbook of Clinical Hepatology*, Vol. 2. Oxford: Oxford University Press, 1991; 1019–52.
5. Shiratori Y, Shiina S, Imamura M *et al.* Characteristic difference of hepatocellular carcinoma between hepatitis B- and C- viral infection in Japan. *Hepatology* 1995; **22**: 1027–33.
6. Yuen MF, Cheng CC, Lauder IJ, Lam SK, Ooi CG, Lai CL. Early detection of hepatocellular carcinoma increases the chance of treatment: Hong Kong experience. *Hepatology* 2000; **31**: 330–5.
7. Bruix J, Sherman M, Llovet JM *et al.* Clinical management of hepatocellular carcinoma. Conclusions of the Barcelona-2000 EASL conference. European Association for the Study of the Liver. *J. Hepatol.* 2001; **35**: 421–30.
8. Kudo M. Early detection and curative treatment of early-stage hepatocellular carcinoma. *Clin. Gastroenterol. Hepatol.* 2005; **3**: S144–8.
9. Ryder SD, British Society of Gastroenterology. Guidelines for the diagnosis and treatment of hepatocellular carcinoma (HCC) in adults. *Gut* 2003; **52**: iii1–8.
10. Llovet JM, Burroughs A, Bruix J. Hepatocellular carcinoma. *Lancet* 2003; **362**: 1907–17.
11. Balsells J, Charco R, Lazaro JL *et al.* Resection of hepatocellular carcinoma in patients with cirrhosis. *Br. J. Surg.* 1996; **83**: 758–61.

12. Mazzaferro V, Regalia E, Doci R *et al.* Liver transplantation for the treatment of small hepatocellular carcinomas in patients with cirrhosis. *N. Engl. J. Med.* 1996; **334**: 693–9.
13. Wall WJ, Marotta PJ. Surgery and transplantation for hepatocellular cancer. *Liver Transpl.* 2000; **6**: S16–22.
14. Vivarelli M, Bellusci R, Cucchetti A *et al.* Low recurrence rate of hepatocellular carcinoma after liver transplantation: Better patient selection or lower immunosuppression? *Transplantation* 2002; **74**: 1746–51.
15. Rossi S, Di Stasi M, Buscarini E *et al.* Percutaneous radio frequency interstitial thermal ablation in the treatment of small hepatocellular carcinoma. *Cancer J. Sci. Am.* 1995; **1**: 73–81.
16. Livraghi T, Goldberg SN, Lazzaroni S, Meloni F, Solbiati L, Gazelle GS. Small hepatocellular carcinoma: Treatment with radiofrequency ablation versus ethanol injection. *Radiology* 1999; **210**: 655–61.
17. Shiina S, Teratani T, Obi S, Hamamura K, Koike Y, Omata M. Nonsurgical treatment of hepatocellular carcinoma: From percutaneous ethanol injection therapy and percutaneous microwave coagulation therapy to radio frequency ablation. *Oncology* 2002; **62**: 64–8.
18. Lencioni RA, Allgaier HP, Cioni D *et al.* Small hepatocellular carcinoma in cirrhosis: Randomized comparison of radiofrequency thermal ablation versus percutaneous ethanol injection. *Radiology* 2003; **228**: 235–40.
19. Curley SA. Radiofrequency ablation of malignant liver tumors. *Oncologist* 2001; **6**: 14–23.
20. Bilchik AJ, Wood TF, Allegra DP. Radiofrequency ablation of unresectable hepatic malignancies: Lessons learned. *Oncologist* 2001; **6**: 24–33.
21. Curley SA, Davidson BS, Fleming RY *et al.* Laparoscopically guided bipolar radiofrequency ablation of areas of porcine liver. *Surg. Endosc.* 1997; **11**: 729–33.
22. Cuschieri A, Bracken J, Boni L. Initial experience with laparoscopic ultrasound-guided radiofrequency thermal ablation of hepatic tumours. *Endoscopy* 1999; **31**: 318–21.
23. Siperstein A, Garland A, Engle K *et al.* Laparoscopic radiofrequency ablation of primary and metastatic liver tumors. Technical considerations. *Surg. Endosc.* 2000; **14**: 400–5.
24. Goletti O, Lencioni R, Armilliotta N *et al.* Laparoscopic radiofrequency thermal ablation of hepatocarcinoma: Preliminary experience. *Surg. Laparosc. Endosc. Percutan. Tech.* 2000; **10**: 284–90.
25. Topal B, Aerts R, Penninckx F. Laparoscopic radiofrequency ablation of unresectable liver malignancies: Feasibility and clinical outcome. *Surg. Laparosc. Endosc. Percutan. Tech.* 2003; **13**: 11–15.
26. Kudo M. Local ablation therapy for hepatocellular carcinoma: Current status and future perspectives. *J. Gastroenterol.* 2004; **39**: 205–14.
27. Patterson EJ, Scudamore CH, Buczkowski AK, Owen DA, Nagy AG. Radiofrequency ablation in surgery. *Surg. Technol. Int.* 1997; **6**: 69–75.
28. Francica G, Marone G. Ultrasound-guided percutaneous treatment of hepatocellular carcinoma by radiofrequency hyperthermia with a 'cooled-tip needle'. A preliminary clinical experience. *Eur. J. Ultrasound.* 1999; **9**: 145–53.
29. Kurokohchi K, Masaki T, Himoto T *et al.* Successful laparoscopic radiofrequency ablation of hepatocellular carcinoma adhered to the mesentery after transcatheter arterial embolization. *Oncol Rep* 2005; **13**: 65–8.
30. Ishiko T, Beppu T, Sugiyama S *et al.* Radiofrequency ablation with hand-assisted laparoscopic surgery for the treatment of hepatocellular carcinoma in the caudate lobe. *Surg. Laparosc. Endosc. Percutan. Tech.* 2008; **18**: 272–6.
31. Belli G, D'Agostino A, Fantini C *et al.* Laparoscopic radiofrequency ablation combined with laparoscopic liver resection for more than one HCC on cirrhosis. *Surg. Laparosc. Endosc. Percutan. Tech.* 2007; **17**: 331–4.
32. Stigliano R, Marelli L, Yu D, Davies N, Patch D, Burroughs AK. Seeding following percutaneous diagnostic and therapeutic approaches for hepatocellular carcinoma. What is the risk and the outcome? Seeding risk for percutaneous approach of HCC. *Cancer Treat. Rev.* 2007; **33**: 437–47.
33. Livraghi T, Solbiati L, Meloni MF, Gazelle GS, Halpern EF, Goldberg SN. Treatment of focal liver tumors with percutaneous radio-frequency ablation: Complications encountered in a multicenter study. *Radiology* 2003; **226**: 441–51.
34. Llovet JM, Vilana R, Brú C *et al.* Increased risk of tumor seeding after percutaneous radiofrequency ablation for single hepatocellular carcinoma. *Hepatology* 2001; **33**: 1124–9.
35. Yokoyama T, Egami K, Miyamoto M *et al.* Percutaneous and laparoscopic approaches of radiofrequency ablation treatment for liver cancer. *J. Hepatobiliary Pancreat. Surg.* 2003; **10**: 425–7.
36. Noguchi O, Izumi N, Kawamura H *et al.* Radiofrequency tumor ablation for hepatocellular carcinoma – Therapeutic significance of approaching methods and the device difference. *Jpn. J. Hyperthermia Oncol.* 2002; **18**: 21–30.
37. Noguchi O, Izumi N, Inoue K *et al.* Laparoscopic ablation therapy for hepatocellular carcinoma. Clinical significance of a newly developed laparoscopic sector ultrasonic probe. *Dig. Endosc.* 2003; **15**: 179–84.
38. Odeberg S, Ljungqvist O, Svenberg T *et al.* Haemodynamic effects of pneumoperitoneum and the influence of posture during anaesthesia for laparoscopic surgery. *Acta Anaesthesiol. Scand.* 1994; **38**: 276–83.
39. Montorsi M, Santambrogio R, Bianchi P *et al.* Laparoscopic radiofrequency of hepatocellular carcinoma (HCC) in liver cirrhosis. *Hepatogastroenterology* 2001; **48**: 41–5.
40. Chung MH, Wood TF, Tsioulias GJ, Rose DM, Bilchik AJ. Laparoscopic radiofrequency ablation of unresectable hepatic malignancies. A phase 2 trial. *Surg. Endosc.* 2001; **15**: 1020–6.
41. Montorsi M, Santambrogio R, Bianchi P *et al.* Radiofrequency interstitial thermal ablation of hepatocellular carcinoma in liver cirrhosis. Role of the laparoscopic approach. *Surg. Endosc.* 2001; **15**: 141–5.
42. Podnos YD, Henry G, Ortiz JA *et al.* Laparoscopic ultrasound with radiofrequency ablation in cirrhotic patients with hepatocellular carcinoma: Technique and technical considerations. *Am. Surg.* 2001; **67**: 1181–4.
43. Santambrogio R, Bianchi P, Palmisano A, Donadon M, Moroni E, Montorsi M. Radiofrequency of hepatocellular carcinoma in patients with liver cirrhosis: A critical appraisal of the laparoscopic approach. *J. Exp. Clin. Cancer. Res.* 2003; **22**: 251–5.
44. Ido K, Nakazawa Y, Isoda N *et al.* The role of laparoscopic US and laparoscopic US-guided aspiration biopsy in the diagnosis of multicentric hepatocellular carcinoma. *Gastrointest. Endosc.* 1999; **50**: 523–6.
45. Salmi A, Metelli F. Laparoscopic ultrasound-guided radiofrequency thermal ablation of hepatic tumors: A new coaxial approach. *Endoscopy* 2003; **35**: 802.
46. Inamori H, Ido K, Isoda N *et al.* Laparoscopic radiofrequency ablation of hepatocellular carcinoma in the caudate lobe by using a new laparoscopic US probe with a forward-viewing convex-array transducer. *Gastrointest. Endosc.* 2004; **60**: 628–31.
47. Hildebrand P, Kleemann M, Roblick UJ, Mirow L, Bürk C, Bruch HP. Technical aspects and feasibility of laparoscopic

ultrasound navigation in radiofrequency ablation of unresectable hepatic malignancies. *J. Laparoendosc. Adv. Surg. Tech. A* 2007; **17**: 53–7.
48. Lai EC, Tang CN, Ha JP, Tsui DK, Li MK. The evolving influence of laparoscopy and laparoscopic ultrasonography on patients with hepatocellular carcinoma. *Am. J. Surg.* 2008; **196**(5): 736–40.
49. Bao P, Sinha TK, Chen CC, Warmath JR, Galloway RL, Herline AJ. A prototype ultrasound-guided laparoscopic radiofrequency ablation system. *Surg. Endosc.* 2007; **21**: 74–9.
50. Raggi MC, Schneider A, Härtl F, Wilhelm D, Wirnhier H, Feussner H. A family of new instruments for laparoscopic radiofrequency ablation of malignant liver lesions. *Minim. Invasive Ther. Allied Technol.* 2006; **15**: 42–7.
51. Abe T, Shinzawa H, Wakabayashi H *et al.* Value of laparoscopic microwave coagulation therapy for hepatocellular carcinoma in relation to tumor size and location. *Endoscopy* 2000; **32**: 598–603.
52. Hildebrand P, Kleemann M, Roblick U, Mirow L, Birth M, Bruch HP. Laparoscopic radiofrequency ablation of unresectable hepatic malignancies: Indication, limitation and results. *Hepatogastroenterology* 2007; **54**: 2069–72.
53. Santambrogio R, Podda M, Zuin M *et al.* Safety and efficacy of laparoscopic radiofrequency ablation of hepatocelluiar carcinoma in patients with liver cirrhosis. *Surg. Endosc.* 2003; **17**: 1826–32.
54. Rossi S, Di Stasi M, Buscarini E *et al.* Percutaneous RF interstitial thermal ablation in the treatment of hepatic cancer. *AJR Am. J. Roentgenol.* 1996; **167**: 759–68.
55. Bowles BJ, Machi J, Limm WM *et al.* Safety and efficacy of radiofrequency thermal ablation in advanced liver tumors. *Arch. Surg.* 2001; **136**: 864–9.
56. Buscarini L, Buscarini E, Di Stasi M, Vallisa D, Quaretti P, Rocca A. Percutaneous radiofrequency ablation of small hepatocellular carcinoma: Long-term results. *Eur. Radiol.* 2001; **11**: 914–21.
57. Curley SA, Izzo F, Delrio P *et al.* Radiofrequency ablation of unresectable primary and metastatic hepatic malignancies: Results in 123 patients. *Ann. Surg.* 1999; **230**: 1–8.
58. Curley SA, Izzo F, Ellis LM, Nicolas Vauthey J, Vallone P. Radiofrequency ablation of hepatocellular cancer in 110 patients with cirrhosis. *Ann. Surg.* 2000; **232**: 381–91.
59. Wood TF, Rose DM, Chung M, Allegra DP, Foshag LJ, Bilchik AJ. Radiofrequency ablation of 231 unresectable hepatic tumors: Indications, limitations, and complications. *Ann. Surg. Oncol.* 2000; **7**: 593–600.
60. Santambrogio R, Opocher E, Costa M, Cappellani A, Montorsi M. Survival and intra-hepatic recurrences after laparoscopic radiofrequency of hepatocellular carcinoma in patients with liver cirrhosis. *J. Surg. Oncol.* 2005; **89**: 218–25.
61. Machi J, Uchida S, Sumida K *et al.* Ultrasound-guided radiofrequency thermal ablation of liver tumors: Percutaneous, laparoscopic, and open surgical approaches. *J. Gastrointest. Surg.* 2001; **5**: 477–89.
62. Topal B, Aerts R, Penninckx F. Laparoscopic radiofrequency ablation of unresectable liver malignancies: Feasibility and clinical outcome. *Surg. Laparosc. Endosc. Percutan. Tech.* 2003; **13**: 11–15.
63. Berber E, Siperstein A. Local recurrence after laparoscopic radiofrequency ablation of liver tumors: An analysis of 1032 tumors. *Ann. Surg. Oncol.* 2008; **15**(10): 2757–64.
64. Izumi N, Asahina Y, Noguchi O *et al.* Risk factors for distant recurrence of hepatocellular carcinoma in the liver after complete coagulation by microwave or radiofrequency ablation. *Cancer* 2001; **91**: 949–56.
65. Berber E, Rogers S, Siperstein A. Predictors of survival after laparoscopic radiofrequency thermal ablation of hepatocellular cancer: A prospective study. *Surg. Endosc.* 2005; **19**: 710–14.
66. Berber E, Siperstein AE. Perioperative outcome after laparoscopic radiofrequency ablation of liver tumors: An analysis of 521 cases. *Surg. Endosc.* 2007; **21**: 613–18.
67. Hsieh CB, Chang HM, Chen TW *et al.* Comparison of transcatheter arterial chemoembolization, laparoscopic radiofrequency ablation, and conservative treatment for decompensated cirrhotic patients with hepatocellular carcinoma. *World J. Gastroenterol.* 2004; **10**: 505–8.
68. Eisele RM, Schumacher G, Jonas S, Neuhaus P. Radiofrequency ablation prior to liver transplantation: Focus on complications and on a rare but severe case. *Clin. Transplant.* 2008; **22**: 20–8.
69. Topal B, Hompes D, Aerts R, Fieuws S, Thijs M, Penninckx F. Morbidity and mortality of laparoscopic vs. open radiofrequency ablation for hepatic malignancies. *Eur. J. Surg. Oncol.* 2007; **33**: 603–7.
70. Pang YY, Andrew YW. Hemoglobinuria during laparoscopic radiofrequency ablation of hepatocellular carcinoma. *J. Gastroenterol. Hepatol.* 2006; **21**: 1355.